7090 J. Med. Chem. 2009, 52, 7090–7102
DOI: 10.1021/jm900871v

Journal of Medicinal Chemistry Article

Synthesis and Evaluation of Three ^{18}F-Labeled Aminophenylbenzothiazoles as Amyloid Imaging Agents

Kim Serdons,*,† Koen Van Laere,‡ Peter Janssen,§ Hank F. Kung,∥ Guy Bormans,† and Alfons Verbruggen†

†*Laboratory for Radiopharmacy, Katholieke Universiteit Leuven, Leuven, Belgium,* ‡*Department of Nuclear Medicine, U.Z. Gasthuisberg, Leuven, Belgium,* §*Department of Neurophysiology, Katholieke Universiteit Leuven, Leuven, Belgium, and* ∥*Department of Radiology, University of Pennsylvania, Pennsylvania*

Received June 15, 2009

We have developed three fluorine-18 labeled 6-(methyl)amino-2-(4′-fluorophenyl)-1,3-benzothiazoles, which display high in vitro binding affinity for human amyloid β plaques ($K_i \leq 10$ nM). The radiolabeled probes were synthesized by aromatic nucleophilic substitution of the corresponding nitro precursor with ^{18}F-fluoride, followed by deprotection of the BOC group if required. Determination of the octanol/water partition coefficient, biodistribution studies in mice, and in vivo μPET studies in rats and a rhesus monkey showed that initial brain uptake was high and brain washout was fast in normal animals. Radiometabolites were quantified in plasma and brain of mice and in monkey plasma using HPLC. Of the tested compounds, [^{18}F]**2** (6-amino-2-(4′-[^{18}F]fluorophenyl)-1,3-benzothiazole) shows the most favorable brain kinetics in mice, rats, and a monkey. Its polar plasma radiometabolites do not cross the blood−brain barrier. The preliminary results strongly suggest that this new fluorinated compound is a promising candidate as a PET brain amyloid imaging agent.

Introduction

Amyloid plaques are one of the pathological hallmarks of Alzheimer's disease (AD[a]), which is a progressive and fatal neurodegenerative brain disorder associated with progressive memory loss and decrease of cognitive functions.[1] The plaques consist of extracellular aggregates of amyloid β (Aβ) peptide and are surrounded by dystrophic axons and dendrites, reactive astrocytes, and activated microglia.[2] Several hypotheses have been postulated to explain the molecular mechanisms leading to AD, but the amyloid cascade hypothesis, stating an imbalance between the production and removal of Aβ, seems to be the most prominent theory at this time.[3] A strong argument supporting a causal role of amyloid in Alzheimer's disease is the fact that new treatment strategies, which are currently in clinical trials, are aimed to delay the disease onset or slow the disease progression by preventing Aβ deposition or increasing Aβ solubilization.[4] Early detection and quantification of the amyloid plaques in brain with noninvasive techniques such as positron emission tomography (PET) would allow not only presymptomatic identification of patients but also monitoring of the effectiveness of these novel treatments.

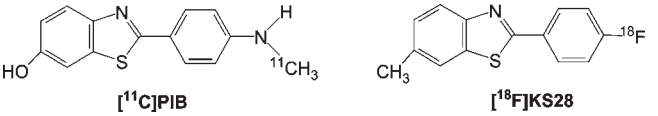

Figure 1. Chemical structures of [^{11}C]PIB and [^{18}F]KS28.

Pittsburgh compound B or [^{11}C]PIB is up to now the most widely used PET radioligand for amyloid visualization in brain.[5,6] However, the short half-life of carbon-11 (20.4 min) restricts the use of [^{11}C]PIB to PET centers equipped with an on-site cyclotron. An ^{18}F-labeled amyloid imaging agent is needed to permit a more widespread application of in vivo amyloid imaging using PET. The longer half-life of fluorine-18 (109.8 min) should provide multiple injections from a single production batch.

Several ^{18}F-labeled tracers for in vivo visualization of amyloid have been proposed,[7−13] and some have been tested in humans. The PIB analogue [^{18}F]KS28 (6-methyl-2-(4′-[^{18}F]fluorophenyl)-1,3-benzothiazole, Figure 1)[14] and the naphthalene derivative [^{18}F]FDDNP,[15] which also labels τ tangles, provide a signal of low specificity. The stilbene derivative [^{18}F]BAY94-9172 shows a similar uptake pattern as [^{11}C]PIB.[16] Mathis et al. also reported a fluorine-18 labeled PIB analogue, which is still under clinical investigation.[17,18]

We have now synthesized and evaluated three new ^{18}F-labeled 2-phenylbenzothiazoles, which all contain a fluorine-18 label directly attached to the 2-phenyl ring and a (methyl substituted) amino group on the benzothiazole part. These electron-donating amino substituents, which are present in all reported promising amyloid tracers, are supposed to contribute significantly to specific in vivo binding to amyloid, as they may increase the binding affinity by introducing a positive electrostatic interaction around the sulfur atom of the phenylbenzothiazole.[19] Their position on the amyloid tracers

*To whom correspondence should be addressed. Phone: +32 16 330441. Fax: +32 16 330449. E-mail: kim.serdons@pharm.kuleuven.be.

[a] Abbreviations: AD, Alzheimer's disease; Aβ, amyloid β; BBB, blood−brain barrier; BOC, butyloxycarbonyl; cpm, counts per minute; DMF, dimethylformamide; DMSO, dimethyl sulfoxide; HPLC, high performance liquid chromatography; ID, injected dose; ID/g, injected dose per gram of tissue; IMPY, 6-iodo-2-(4′-dimethylamino)phenylimidazo[1,2]pyridine; LSO, lutetium oxyorthosilicate; MCI, mild cognitive impairment; Mp, melting point; NMR, nuclear magnetic resonance; *P*, partition coefficient; PBS, phosphate buffered saline; p.i., postinjection; PET, positron emission tomography; RP-HPLC, reversed phase high performance liquid chromatography; ROI, region of interest; t_R, retention time; rt, room temperature; SD, standard deviation; SEM, standard error of the mean; SUV, standard uptake value; TAC, time−activity curve; THF, tetrahydrofuran; TLC, thin layer chromatography; VOI, volume of interest.

 Published on Web 10/30/2009

seems to have no influence on the binding characteristics. We here report the synthesis, radiolabeling, in vitro affinity, and in vivo biological evaluation in normal mice, rat, and monkey of three new ^{18}F-labeled 2-phenylbenzothiazoles.

Results and Discussion

Chemistry. All described 2-fluorophenyl- or 2-nitrophenyl-1,3-benzothiazoles were synthesized by direct coupling of the corresponding benzothiazoles with the aryl bromide 1-bromo-4-fluorobenzene or 1-bromo-4-nitrobenzene, respectively (Schemes 1−3).[20] The yields of this one-step reaction varied between 3% and 41%.

Scheme 1. Synthesis of 6-Amino-2-(4′-fluorophenyl)-1,3-benzothiazole (**2**) and 6-Methylamino-2-(4′-fluorophenyl)-1,3-benzothiazole (**3**)[a]

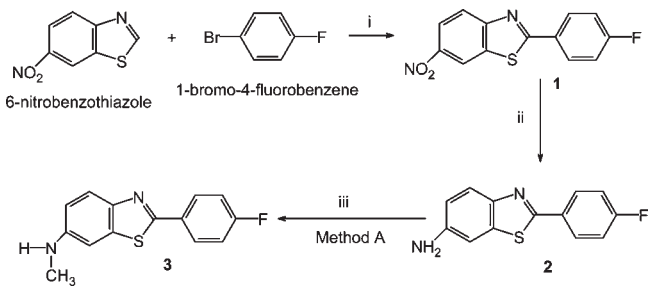

[a] (i) Cs_2CO_3, CuBr, $Pd(OAc)_2$, P(*t*-Bu)$_3$, DMF, 150 °C, 3 h; (ii) $SnCl_2 \cdot 2H_2O$, ethanol, reflux, 4 h; (iii) method A, sodium methoxide, paraformaldehyde, sodium borohydride, methanol, reflux, 3 h.

The nitro group of 6-nitro-2-(4′-fluorophenyl)-1,3-benzothiazole (**1**) was reduced with Sn^{2+} ions in ethanol, and the resulting 6-amino-2-(4′-fluorophenyl)-1,3-benzothiazole (**2**) was monomethylated using the deprotonating agent sodium methoxide, paraformaldehyde, and the reducing agent sodium borohydride in methanol (Scheme 1, method A).[21] 6-Methylamino-2-(4′-fluorophenyl)-1,3-benzothiazole (**3**) was also synthesized by direct coupling of 6-methylaminobenzothiazole (**10**) with 1-bromo-4-fluorobenzene with a yield of 17% (method B).

6-Dimethylamino-2-(4′-fluorophenyl)-1,3-benzothiazole (**6**) and precursor 6-dimethylamino-2-(4′-nitrophenyl)-1,3-benzothiazole (**7**) were synthesized starting from 6-dimethylaminobenzothiazole (**5**), which was obtained by reduction of 6-nitrobenzothiazole (Scheme 2)[22] followed by dimethylation using formaldehyde in the presence of sulfuric acid and powdered iron.[23]

The precursors 6-*tert*-butoxycarbonylamino-2-(4′-nitrophenyl)-1,3-benzothiazole (**9**) and 6-*tert*-butoxycarbonylmethylamino-2-(4′-nitrophenyl)-1,3-benzothiazole (**12**) were synthesized by direct coupling of 1-bromo-4-nitrobenzene with 6-*tert*-butoxycarbonylaminobenzothiazole (**8**) or 6-*tert*-butoxycarbonylmethylaminobenzothiazole (**11**), respectively

Scheme 2. Synthesis of 6-Dimethylamino-2-(4′-fluorophenyl)-1,3-benzothiazole (**6**) and 6-Dimethylamino-2-(4′-nitrophenyl)-1,3-benzothiazole (**7**)[a]

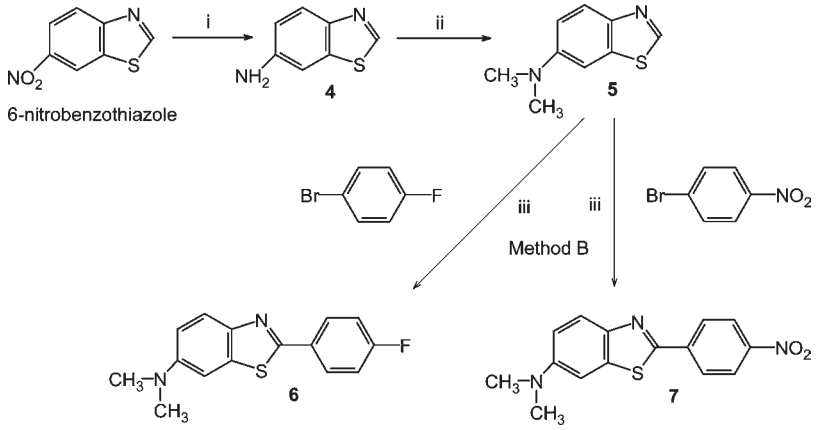

[a] (i) $SnCl_2 \cdot 2H_2O$, concentrated HCl, methanol, reflux, 30 min; (ii) H_2SO_4, Fe, formaldehyde, THF, reflux, 30 min; (iii) method B, Cs_2CO_3, CuBr, $Pd(OAc)_2$, P(*t*-Bu)$_3$, DMF, 150 °C, 30 min.

Scheme 3. Synthesis of 6-*tert*-Butoxycarbonylamino-2-(4′-nitrophenyl)-1,3-benzothiazole (**9**) and 6-*tert*-Butoxycarbonylmethylamino-2-(4′-nitrophenyl)-1,3-benzothiazole (**12**)[a]

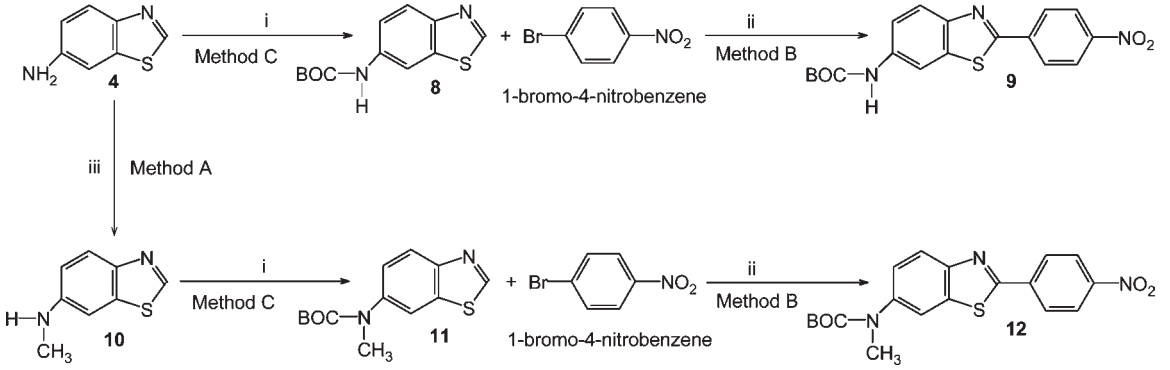

[a] (i) Method C, $Zn(ClO_4)_2 \cdot 6H_2O$, $(BOC)_2O$, *tert*-butanol, 80 °C, 3 h; (ii) method B, Cs_2CO_3, CuBr, $Pd(OAc)_2$, P(*t*-Bu)$_3$, DMF, 150 °C, 30 min; (iii) method A, sodium methoxide, paraformaldehyde, sodium borohydride, reflux, 3 h.

Scheme 4. Synthesis of 6-Amino-2-(4′-[^{18}F]fluorophenyl)-1,3-benzothiazole [^{18}F]**2**, 6-Methylamino-2-(4′-[^{18}F]fluorophenyl)-1,3-benzothiazole [^{18}F]**3**, and 6-Dimethylamino-2-(4′-[^{18}F]fluorophenyl)-1,3-benzothiazole [^{18}F]**6**[a]

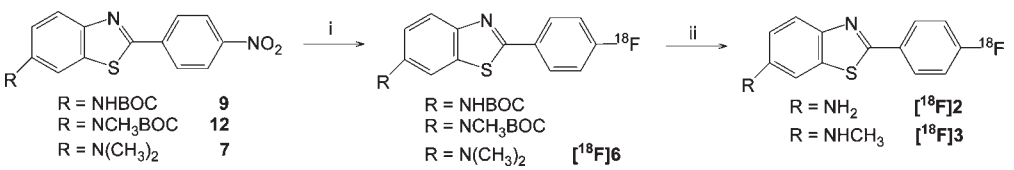

[a] (i) $^{18}F^-$, K_2CO_3, Kryptofix, DMSO, 150 °C, 20 min; (ii) 1 M HCl, 100 °C, 5 min.

Table 1. K_i Values for Human Amyloid, log *P* Values, and Radiochemical Characteristics of **2**, **3**, **6**, KS28, and PIB

compd	K_i[a] (nM)	log *P*[b]	t_R of nitro precursor (min)	t_R of ^{18}F/F product (min)	radiochemical yield[g] (%)
2	10.0 ± 1.0	3.08 ± 0.04	9[c]	7.5[c]	10.5 ± 5.2
3	4.1 ± 0.3	2.40 ± 0.30	8[d]	12[d]	45.0 ± 12.5
6	3.8 ± 0.4	3.34 ± 0.13	11[e]	7.5[e]	19.3 ± 9.0
KS28	5.7 ± 1.8	2.52 ± 0.27	48[f]	41[f]	29.4 ± 3.2
PIB	2.8 ± 0.5	2.48 ± 0.06	nd[h]	nd[h]	nd[h]

[a] K_i expressed as mean ± SEM (standard error of the mean) in an [^{125}I]IMPY competition study (K_d([^{125}I]IMPY) = 5.3 ± 1.0 nM). [b] log *P* expressed as mean ± SD (standard deviation, n = 6). [c] t_R (retention time) determined on HPLC. Stationary phase: XTerra Prep RP_{18} (3.5 μm, 3.0 mm × 100 mm). Mobile phase: 0.05 M ammonium acetate and ethanol/THF (75:25) (60:40 v/v and after 5 min 40:60 v/v). Flow rate: 0.35 mL/min. Detection: UV 254 nm. [d] t_R (retention time) determined on HPLC. Stationary phase: XTerra Prep RP_{18} (3.5 μm, 3.0 mm × 100 mm). Mobile phase: 0.05 M ammonium acetate and ethanol/THF (75:25) (55:45 v/v). Flow rate: 0.35 mL/min. Detection: UV 254 nm. [e] t_R (retention time) determined on HPLC. Stationary phase: XTerra Prep RP_{18} (3.5 μm, 3.0 mm × 100 mm). Mobile phase: 0.05 M ammonium acetate and ethanol/THF (75:25) (45:55 v/v). Flow rate: 0.35 mL/min. Detection: UV 254 nm. [f] t_R (retention time) determined on HPLC. Stationary phase: XTerra Prep RP_{18} (10 μm, 10 mm × 250 mm). Mobile phase: 0.05 M ammonium acetate and ethanol/THF (75:25) (50:50 v/v). Flow rate: 3 mL/min. Detection: UV 234 nm. [g] Decay corrected radiochemical yield expressed as mean ± SD (standard deviation, n > 7). [h] nd = not determined.

(Scheme 3). The butyloxycarbonyl (BOC) protecting group of these benzothiazoles was introduced on the amino or methylamino group of 6-aminobenzothiazole (**4**) or 6-methylaminobenzothiazole (**10**), respectively, using the mild Lewis acid zinc perchlorate hexahydrate as catalyst.[24] Several attempts to introduce the BOC-protecting group directly on the 6-aminophenylbenzothiazole failed. **10** was synthesized starting from **4** using the selective monomethylation method (method A).

The overall yields of the synthesis pathways depicted in Schemes 1−3 were rather low (< 10%), but several other attempts to synthesize the described 2-phenyl-1,3-benzothiazoles **2**, **3**, **6**, **7**, **9**, and **12** failed. Synthesis of the phenylbenzothiazoles by direct coupling of the corresponding thiophenol with 4-nitrobenzoic acid or 4-fluorobenzoic acid in polyphosphoric acid[25] appeared not possible, as the synthesis of the required thiophenols was not successful. Synthesis of the phenylbenzothiazoles **2**, **6**, **7**, and **9** via the three-step pathway as described previously[26] failed because the final ring closure using $K_3Fe(CN)_6$ in 10% NaOH was not successful.

Radiochemistry. To introduce the ^{18}F-label on the 2-phenyl ring of the phenylbenzothiazoles, an aromatic nucleophilic substitution of a [^{18}F]fluorine atom for the nitro group was achieved by heating the solution of the precursor with K[^{18}F]F-Kryptofix complex in dimethyl sulfoxide (DMSO) at 150 °C for 20 min.[25] Radiolabeling of 6-amino-2-(4′-nitrophenyl)-1,3-benzothiazole and 6-methylamino-2-(4′-nitrophenyl)-1,3-benzothiazole failed probably because in the alkaline labeling conditions a partial negative charge is induced on the N-atom at position 6. As a result, the benzothiazole substituent no longer acts as electron-withdrawing substituent and replacement of the 4′-nitro group by [^{18}F]fluoride using a nucleophilic substitution reaction is not possible. To overcome this problem, we introduced a BOC protecting group on the amine at position 6. Labeling of these precursors, 6-*tert*-butoxycarbonylamino-2-(4′-nitrophenyl)-1,3-benzothiazole (**9**) and 6-*tert*-butoxycarbonylmethylamino-2-(4′-nitrophenyl)-1,3-benzothiazole (**12**), resulted in the corresponding fluorine-18 radiolabeled 6-amino-2-(4′-[^{18}F]fluorophenyl)-1,3-benzothiazole ([^{18}F]**2**) and 6-methylamino-2-(4′-[^{18}F]fluorophenyl)-1,3-benzothiazole ([^{18}F]**3**) after removal of the BOC-protecting group with 1 M hydrochloric acid (Scheme 4). The crude mixtures were purified using preparative reversed phase HPLC (RP-HPLC). The tetrahydrofuran (THF) present in the HPLC eluent was removed by solid phase extraction using a Sep-Pak Plus C18 cartridge.

Radiolabeling of the BOC-protected precursors using a microwave cavity was not successful, as the BOC group was found to be removed prior to the nucleophilic substitution. Radiolabeling of dimethylaminonitrophenylbenzothiazole **7** using a microwave cavity surprisingly resulted in lower yields compared to conventional heating.

The purified tracer products were analyzed on an analytical C_{18} column, and their radiochemical purity was found to be more than 99%. The identity of the tracers was confirmed by coelution with the authentic nonradioactive compounds after co-injection on the same analytical HPLC system.

Affinity. The in vitro affinity of the nonradioactive reference compounds for amyloid β fibrils was determined using an [^{125}I]IMPY binding competition experiment with human AD brain homogenates.[27] All compounds (**2**, **3**, and **6**) were found to have a low K_i value (≤10 nM) and thus show good affinity for Aβ plaques (Table 1).

Partition Coefficient. As an estimate of the potential of the compounds to cross the blood−brain barrier (BBB) by passive diffusion, the lipophilicity of the RP-HPLC purified radiolabeled products was determined by partitioning between 1-octanol and 0.025 M phosphate buffer, pH 7.4 (n = 6). The log of the partition coefficient (P) values of [^{18}F]**2**, [^{18}F]**3**, and [^{18}F]**6** were 3.08 ± 0.04, 2.40 ± 0.30 and 3.34 ± 0.13, respectively (Table 1). The log *P* values of [^{18}F]**2** and [^{18}F]**6** are slightly higher than the optimal value (log *P* between 1 and 3) for passive diffusion of a compound through the BBB.[28]

Table 2. Tissue Distribution of 6-Amino-2-(4′-[^{18}F]fluorophenyl)-1,3-benzothiazole ([^{18}F2) after iv Injection in Normal Mice at 2 and 60 min p.i.[a]

	% ID ± SD		% ID/g tissue ± SD		SUV ± SD	
organ	2 min p.i.	60 min p.i.	2 min p.i.	60 min p.i.	2 min p.i.	60 min p.i.
urine	0.2 ± 0.1	4.9 ± 1.1				
kidneys	8.3 ± 0.5	1.0 ± 0.3	13.3 ± 1.2	1.8 ± 0.5	4.2 0.3	0.6 0.2
liver	39.8 ± 2.3	10.7 ± 1.1	20.0 ± 3.6	5.6 ± 0.6	6.4 ± 0.9	1.8 ± 0.2
spleen + pancreas	1.4 ± 0.2	0.3 ± 0.0	6.8 ± 0.6	1.1 ± 0.1	2.2 ± 0.2	0.3 ± 0.0
lungs	2.0 ± 0.4	0.3 ± 0.1	8.9 ± 1.4	1.2 ± 0.1	2.8 ± 0.4	0.4 ± 0.0
heart	0.7 ± 0.1	0.1 ± 0.0	5.9 ± 0.4	0.7 ± 0.1	1.9 ± 0.1	0.2 ± 0.0
intestines	11.1 ± 1.2	68.6 ± 3.2				
stomach	1.6 ± 0.2	0.6 ± 0.5				
cerebrum	4.56 ± 0.16	0.32 ± 0.04	13.97 ± 0.63	0.97 ± 0.17	4.47 ± 0.10	0.31 ± 0.05
cerebellum	1.74 ± 0.41	0.17 ± 0.07	15.48 ± 0.59	1.34 ± 0.31	4.96 ± 0.16	0.42 ± 0.10
blood	5.3 ± 2.2	1.3 ± 0.7	2.4 ± 0.9	0.6 ± 0.3	0.8 ± 0.3	0.2 ± 0.1

[a] $n = 4$ at each time point.

Table 3. Tissue Distribution of 6-Methylamino-2-(4′-[^{18}F]fluorophenyl)-1,3-benzothiazole ([^{18}F]**3**) after iv Injection in Normal Mice at 2 and 60 min p.i.[a]

	% ID ± SD		% ID/g tissue ± SD		SUV ± SD	
organ	2 min p.i.	60 min p.i.	2 min p.i.	60 min p.i.	2 min p.i.	60 min p.i.
urine	0.2 ± 0.1	13.0 ± 3.3				
kidneys	8.2 ± 0.5	3.2 ± 1.3	12.6 ± 0.7	4.6 ± 1.6	4.3 ± 0.6	1.6 ± 0.5
liver	42.4 ± 3.0	17.5 ± 6.1	20.8 ± 1.5	8.3 ± 3.9	7.0 ± 0.7	2.8 ± 1.2
spleen + pancreas	1.4 ± 0.2	0.3 ± 0.1	5.9 ± 0.3	0.9 ± 0.4	2.0 ± 0.2	0.3 ± 0.1
lungs	1.8 ± 0.4	0.3 ± 0.1	7.3 ± 0.9	1.4 ± 0.4	2.5 ± 0.4	0.5 ± 0.1
heart	0.8 ± 0.2	0.2 ± 0.1	5.8 ± 1.0	1.0 ± 0.3	2.0 ± 0.3	0.4 ± 0.1
intestines	11.0 ± 0.5	37.2 ± 10.8				
stomach	2.3 ± 0.6	1.6 ± 1.8				
cerebrum	3.42 ± 0.25	0.44 ± 0.13	12.13 ± 0.48	1.39 ± 0.23	4.10 ± 0.53	0.48 ± 0.08
cerebellum	1.19 ± 0.44	0.12 ± 0.05	11.76 ± 0.66	1.26 ± 0.25	3.97 ± 0.42	0.44 ± 0.13
blood	1.5 ± 1.3	2.2 ± 1.6	0.7 ± 0.6	0.9 ± 0.7	0.2 ± 0.2	0.3 ± 0.2

[a] $n = 4$ at each time point.

Table 4. Tissue Distribution of 6-Dimethylamino-2-(4′-[^{18}F]fluorophenyl)-1,3-benzothiazole ([^{18}F]**6**) after iv Injection in Normal Mice at 2 and 60 min p.i.[a]

	% ID ± SD		% ID/g tissue ± SD		SUV ± SD	
organ	2 min p.i.	60 min p.i.	2 min p.i.	60 min p.i.	2 min p.i.	60 min p.i.
urine	0.1 ± 0.0	7.6 ± 2.6				
kidneys	8.5 ± 0.6	4.8 ± 1.9	11.7 ± 0.8	6.5 ± 2.5	4.3 ± 0.4	2.4 ± 0.9
liver	41.9 ± 4.1	18.9 ± 2.6	18.9 ± 1.0	8.0 ± 1.2	6.8 ± 0.1	3.0 ± 0.4
spleen + pancreas	1.5 ± 0.1	0.3 ± 0.1	5.5 ± 0.7	1.0 ± 0.1	2.0 ± 0.2	0.4 ± 0.0
lungs	2.2 ± 0.3	0.6 ± 0.2	8.0 ± 0.9	1.9 ± 0.3	2.9 ± 0.5	0.7 ± 0.1
heart	1.2 ± 0.1	0.2 ± 0.0	7.4 ± 0.7	1.3 ± 0.2	2.7 ± 0.1	0.5 ± 0.1
intestines	10.0 ± 0.6	28.0 ± 3.6				
stomach	1.4 ± 0.2	1.2 ± 1.3				
cerebrum	2.95 ± 0.33	0.65 ± 0.06	8.84 ± 0.91	1.94 ± 0.20	3.20 ± 0.23	0.72 ± 0.08
cerebellum	0.77 ± 0.39	0.22 ± 0.10	9.23 ± 0.29	2.24 ± 0.56	3.35 ± 0.22	0.83 ± 0.21
blood	2.8 ± 1.3	2.4 ± 0.2	1.1 ± 0.6	0.9 ± 0.1	0.4 ± 0.2	0.3 ± 0.0

[a] $n = 4$ at each time point.

Biodistribution in Normal Mice. A biodistribution study of [^{18}F]**2**, [^{18}F]**3**, and [^{18}F]**6** was performed in normal male NMRI mice at 2 and 60 min postinjection (p.i.) to assess the brain pharmacokinetics. Tables 2, 3, and 4 list the tracer uptake in the most important organs. All compounds showed a very high initial brain uptake. The initial uptake in cerebrum of [^{18}F]**2** is the highest of the three compounds (13.97 ± 0.63% ID/g). [^{18}F]**3** and [^{18}F]**6** show an initial uptake in the cerebrum of 12.13 ± 0.48% ID/g and 8.84 ± 0.91% ID/g, respectively. Brain uptake of all three compounds at 2 min p.i. is significantly higher ($p < 0.05$, two-sided) than that of [^{11}C]PIB (Table 5, 3.60 ± 1.40% ID/g) and [^{18}F]KS28 (Table 6, 5.33 ± 0.74% ID/g). Brain uptake of [^{18}F]**2** is significantly higher ($p < 0.05$, two-sided) than that of [^{18}F]**3** and [^{18}F]**6**, and brain uptake of [^{18}F]**3** is significantly higher ($p < 0.05$, two-sided) than that of [^{18}F]**6**. With respect to brain washout (expressed as the ratio of % ID in cerebrum at 2 min over % ID in cerebrum at 60 min), [^{18}F]**2** shows a higher value (14.2) than [^{18}F]**3** (7.8) and [^{18}F]**6** (4.5). In healthy mice, a compound with favorable characteristics for plaque imaging not only should have a high affinity for amyloid but also should show a high initial brain uptake followed by a rapid washout, indicating absence of nonspecific binding to any brain structure devoid of amyloid plaques. On the basis of these results, compound [^{18}F]**2** seems to be the compound with the most promising characteristics to image AD in vivo in view of the highest initial brain uptake, which is 4 times higher than that of [^{11}C]PIB and almost 3 times higher than that of [^{18}F]KS28, and the fastest brain washout value. We also studied the biodistribution of [^{18}F]**2** at 60 min p.i. in mice pretreated with reference compound **2**. There was no significant difference ($p < 0.05$, two-sided) between the

Table 5. Tissue Distribution of 6-Hydroxy-2-(4′-N-[^{11}C]methylaminophenyl)-1,3-benzothiazole ([^{11}C]PIB) after iv Injection in Normal Mice at 2 and 60 min p.i.[a]

	% ID ± SD		% ID/g tissue ± SD		SUV ± SD	
organ	2 min p.i.	60 min p.i.	2 min p.i.	60 min p.i.	2 min p.i.	60 min p.i.
urine	0.2 ± 0.1	24.4 ± 10.1				
kidneys	10.3 ± 3.8	4.8 ± 3.9	19.9 ± 9.1	9.1 ± 7.1	7.4 ± 2.6	3.3 ± 2.6
liver	15.6 ± 4.5	9.8 ± 2.6	7.9 ± 2.6	5.0 ± 1.7	2.9 ± 0.6	1.8 ± 0.6
spleen + pancreas	0.6 ± 0.1	0.1 ± 0.1	4.7 ± 2.4	0.7 ± 0.4	1.8 ± 0.2	0.2 ± 0.2
lungs	0.9 ± 0.2	0.3 ± 0.2	3.6 ± 0.6	1.3 ± 0.7	1.3 ± 0.2	0.4 ± 0.2
heart	0.6 ± 0.1	0.3 ± 0.2	4.2 ± 0.3	2.1 ± 2.1	1.5 ± 0.7	0.7 ± 0.7
intestines	12.0 ± 2.4	42.5 ± 7.5				
stomach	1.1 ± 0.2	0.3 ± 0.2				
cerebrum	1.08 ± 0.44	0.18 ± 0.06	3.60 ± 1.40	0.60 ± 0.21	1.33 ± 0.08	0.22 ± 0.08
cerebellum	0.17 ± 0.02	0.03 ± 0.02	1.60 ± 0.09	0.31 ± 0.13	0.59 ± 0.05	0.11 ± 0.05
blood	7.9 ± 0.5	2.7 ± 0.8	3.1 ± 0.2	1.1 ± 0.3	1.13 ± 0.11	0.4 ± 0.1

[a] $n = 6$ at each time point.

Table 6. Tissue Distribution of 6-Methyl-2-(4′-[^{18}F]fluorophenyl)-1,3-benzothiazole ([^{18}F]KS28) after iv Injection in Normal Mice at 2 and 60 min p.i.[a]

	% ID ± SD		% ID/g tissue ± SD		SUV ± SD	
organ	2 min p.i.	60 min p.i.	2 min p.i.	60 min p.i.	2 min p.i.	60 min p.i.
urine	0.2 ± 0.1	3.3 ± 1.8				
kidneys	5.8 ± 1.4	2.3 ± 0.2	9.3 ± 2.0	3.6 ± 0.4	3.4 ± 0.8	1.4 ± 0.1
liver	24.8 ± 3.3	51.8 ± 1.8	12.0 ± 0.7	24.6 ± 2.1	4.5 ± 0.5	9.2 ± 0.7
spleen + pancreas	1.3 ± 0.2	0.1 ± 0.0	4.0 ± 0.7	0.4 ± 0.1	1.5 ± 0.2	0.2 ± 0.0
lungs	3.6 ± 1.0	0.3 ± 0.1	14.4 ± 2.0	1.3 ± 0.2	5.3 ± 0.7	0.5 ± 0.1
heart	0.9 ± 0.1	0.1 ± 0.0	5.4 ± 0.5	0.5 ± 0.1	2.0 ± 0.1	0.2 ± 0.0
intestines	8.9 ± 1.0	19.3 ± 1.3				
stomach	1.3 ± 0.2	1.1 ± 0.6				
cerebrum	1.62 ± 0.29	0.07 ± 0.02	5.33 ± 0.74	0.27 ± 0.06	1.97 ± 0.29	0.10 ± 0.02
cerebellum	0.42 ± 0.16	0.04 ± 0.02	5.99 ± 0.70	0.39 ± 0.06	2.21 ± 0.23	0.15 ± 0.03
blood	5.7 ± 2.4	2.8 ± 2.2	2.2 ± 0.9	1.1 ± 0.9	0.8 ± 0.4	0.4 ± 0.3

[a] $n = 6$ at each time point.

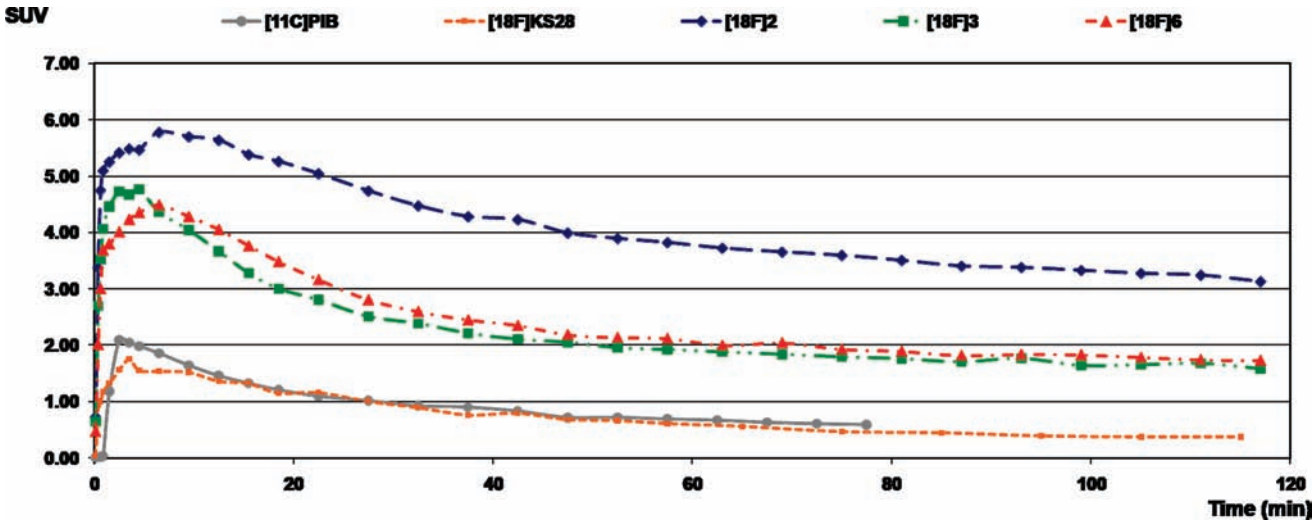

Figure 2. Standard uptake values (SUVs) of [^{11}C]PIB, [^{18}F]KS28, [^{18}F]**2**, [^{18}F]**3**, and [^{18}F]**6** in the frontotemporal cortex of a normal rat.

biodistribution values of the untreated and pretreated mice, indicating that the residual brain activity of [^{18}F]**2** at 60 min p.i. is due to nonspecific binding.

Blood levels of the three compounds were relatively low at all time points measured. The clearance of [^{18}F]**2** from blood (expressed as the ratio % ID in blood at 2 min over % ID in blood at 60 min, 4.1) was faster than that of [^{11}C]PIB (2.9) and [^{18}F]KS28 (2.0). As can be expected from the relatively high log *P* value, the compounds were cleared from plasma mainly by the hepatobiliary system (ranging from 47% ID in liver and intestines for the dimethylamino derivative to 79% ID for the amino derivative at 60 min p.i.). Only a small fraction of the radioactivity was excreted with the urine (ranging from 5.9% ID for the amino derivative to 16% ID for the methylamino derivative at 60 min p.i.). In accordance with previous reports,[29] there is no real correlation between the lipophilicity of the compounds (log *P*) and the degree of renal or hepatobiliary clearance. Except for the liver, intestines, and kidneys, the amount of radioactivity in other major organs was negligible 60 min after injection of the tracers.

***μ*PET Study in a Normal Rat.** To compare the brain pharmacokinetics of [^{18}F]**2**, [^{18}F]**3**, and [^{18}F]**6** with those of

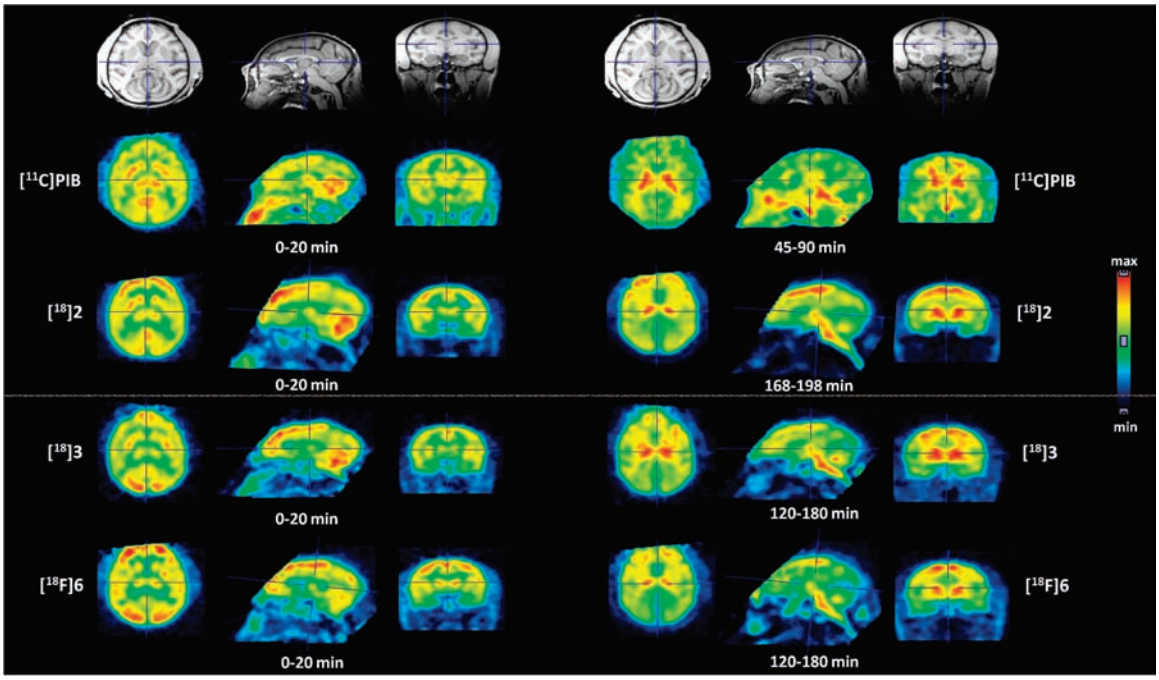

Figure 3. Dynamic μPET study of [^{11}C]PIB, [^{18}F]**2**, [^{18}F]**3**, and [^{18}F]**6** in a normal rhesus monkey. Transverse, sagittal, and coronal MRI and summed PET images between 0 and 20 min p.i. (left) and between 45 and 90 min p.i. for [^{11}C]PIB, between 168 and 198 min for [^{18}F]**2**, and between 120 and 180 min p.i. for [^{18}F]**3** and [^{18}F]**6** (right).

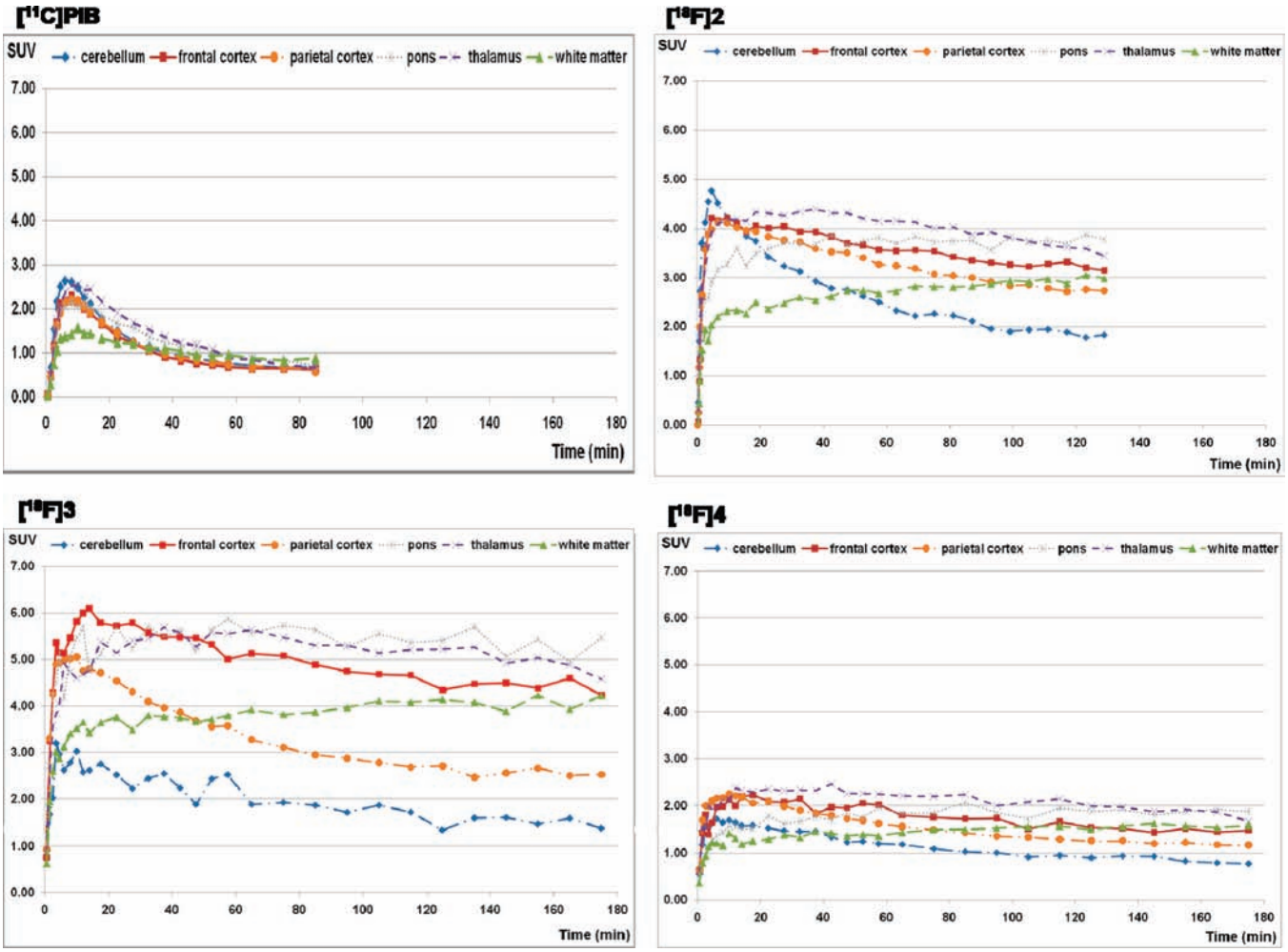

Figure 4. Standard uptake values (SUVs) of [^{11}C]PIB, [^{18}F]**2**, [^{18}F]**3**, and [^{18}F]**6** in the cerebellum, frontal cortex, parietal cortex, pons, thalamus, and white matter of a normal rhesus monkey.

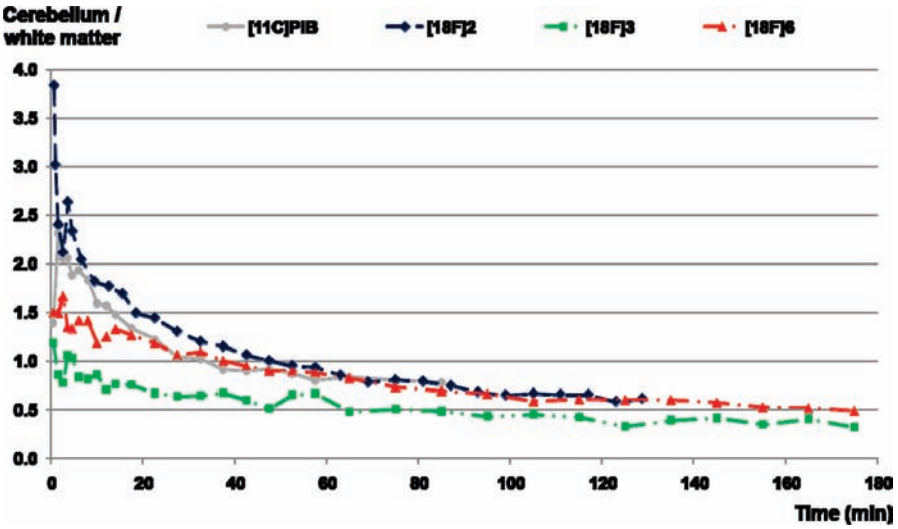

Figure 5. Ratio cerebellum/white matter of [^{11}C]PIB, [^{18}F]**2**, [^{18}F]**3**, and [^{18}F]**6** in a normal rhesus monkey.

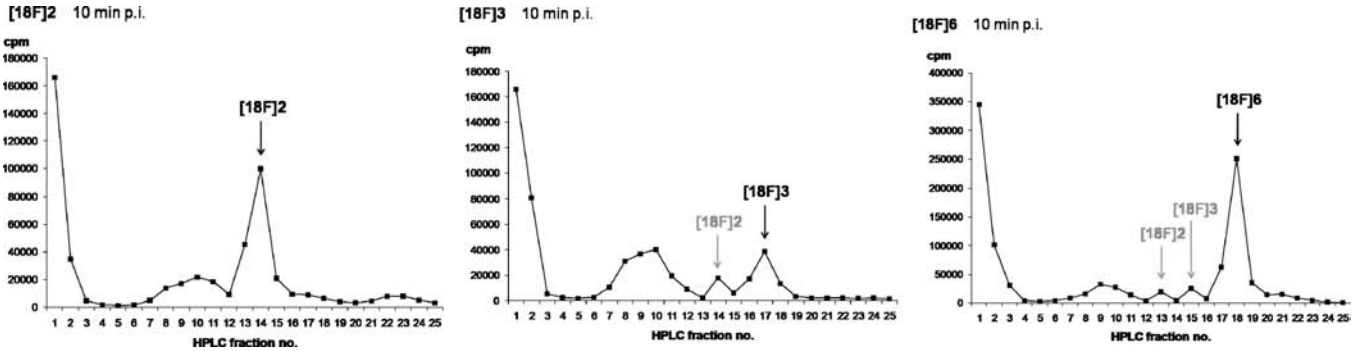

Figure 6. Plasma radiometabolite analysis of [^{18}F]**2**, [^{18}F]**3**, and [^{18}F]**6**: RP-HPLC radiochromatogram of a plasma sample from a normal mouse collected at 10 min p.i. The 1 min fractions were collected and counted.

[^{11}C]PIB and [^{18}F]KS28, the compounds were injected in a normal rat and brain μPET images were acquired for 120 min. Figure 2 shows the time−activity curves (TACs) for [^{11}C]PIB, [^{18}F]KS28, [^{18}F]**2**, [^{18}F]**3**, and [^{18}F]**6** in the frontotemporal cortex of a normal rat. Values are expressed as standard uptake values (SUVs).

The three new fluorine-18 labeled PIB derivatives all showed an initial brain uptake more than 2 times higher than that of [^{11}C]PIB and [^{18}F]KS28. When we compare the SUV values of mice (cerebrum, Tables 1−6) and rats (frontotemporal cortex), we see that the relative proportion of initial tracer uptake was identical for [^{18}F]**2**, [^{18}F]**3**, and [^{18}F]**6**. However, when we compare the brain activity present at 60 min p.i., we see that the values of [^{18}F]**2**, [^{18}F]**3**, and [^{18}F]**6** in the cerebrum of mice are lower than the values in the frontotemporal cortex of the rat. This slower clearance of the fluorine-18 labeled aminophenylbenzothiazoles in rats may be explained by interspecies differences.

As no tracer uptake was observed in the skull, we can conclude that the new ^{18}F-labeled 2-phenylbenzothiazoles do not show substantial defluorination in vivo.

In a pretreatment study a rat was intraperitoneally injected with reference compound **2** (0.35 mg) 30 min prior to iv injection of [^{18}F]**2**. Similar to the biodistribution study in mice, there was no significant difference ($p < 0.05$, two-sided) between the SUV values of this pretreated rat and the untreated rat, indicating that brain retention of [^{18}F]**2** is nonspecific.

Table 7. Percentage of Intact [^{18}F]KS28, [^{18}F]**2**, [^{18}F]**3**, and [^{18}F]**6** ± SD in Plasma of Normal Mice at 2, 10, 30, and 60 min p.i.[a]

	% intact tracer in plasma mice			
	2 min p.i.	10 min p.i.	30 min p.i.	60 min p.i.
[^{18}F]KS28[b]	52.2 ± 13.2	14.0 ± 6.2	7.9 ± 2.8	3.2 ± 1.7
[^{18}F]**2**[c]	70.0 ± 5.4	41.7 ± 4.9	33.4 ± 7.1	16.5 ± 2.0
[^{18}F]**3**[c]	54.4 ± 13.3	17.4 ± 3.4	7.9 ± 2.4	4.1 ± 1.4
[^{18}F]**6**[c]	77.0 ± 3.8	37.0 ± 1.1	7.7 ± 2.7	6.0 ± 6.4

[a] $n = 3$ at each time point. [b] Plasma samples were analyzed on an Oasis HLB column (25 μm, 4.6 mm × 20 mm, Waters). [c] Plasma samples were analyzed on a Chromolith Performance RP-18 column (3 mm × 100 mm, Merck).

μPET Study in a Normal Rhesus Monkey. Because of the observed interspecies differences between mice and rats with regard to the brain washout of the studied compounds and to demonstrate a high initial brain uptake in nonhuman primates, we decided to further evaluate the three new ^{18}F-labeled phenylbenzothiazoles in a normal rhesus monkey prior to selection of a compound for further clinical evaluation. Brain μPET images were acquired for 180 min for the ^{18}F compounds [^{18}F]**2**, [^{18}F]**3**, and [^{18}F]**6** and for 90 min for [^{11}C]PIB. Figure 3 shows the MRI and summed PET images between 0 and 20 min p.i. for [^{11}C]PIB, [^{18}F]**2**, [^{18}F]**3**, and [^{18}F]**6** (left) and between 45 and 90 min p.i. for [^{11}C]PIB and 120 and 180 min p.i. for [^{18}F]**3** and [^{18}F]**6** (right). Note that because of technical reasons for [^{18}F]**2** the

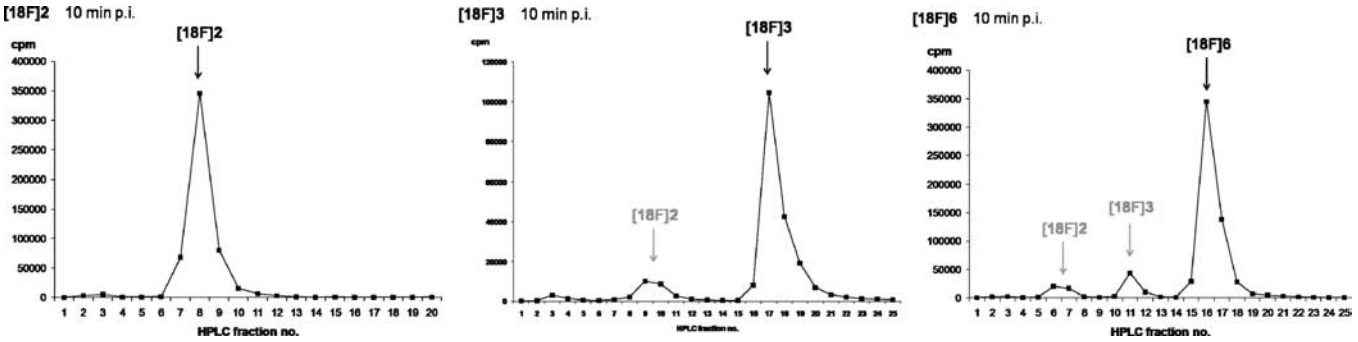

Figure 7. Brain radiometabolite analysis of [^{18}F]**2**, [^{18}F]**3**, and [^{18}F]**6**: RP-HPLC radiochromatogram of a brain sample from a normal mouse collected at 10 min p.i. The 1 min fractions were collected and counted.

Table 8. Percentage of Intact [^{18}F]KS28, [^{18}F]**2**, [^{18}F]**3**, and [^{18}F]**6** ± SD in Brain of Normal Mice at 2, 10, 30, and 60 min p.i.[a]

	% intact tracer brain mice			
	2 min p.i.	10 min p.i.	30 min p.i.	60 min p.i.
[^{18}F]KS28	89.2 ± 0.4	nd	nd	86.2 ± 2.5
[^{18}F]**2**	98.8 ± 0.5	97.7 ± 0.5	94.8 ± 1.8	86.3 ± 0.0
[^{18}F]**3**	92.7 ± 1.0	84.0 ± 3.3	69.1 ± 4.0	60.3 ± 3.9
[^{18}F]**6**	90.4 ± 1.8	79.9 ± 5.4	68.7 ± 17.6	59.2 ± 17.9

[a] [^{18}F]KS28: $n = 2$ at each time point. [^{18}F]**2**, [^{18}F]**3**, and [^{18}F]**6**: $n = 3$ at each time point. nd = not determined.

Table 9. Percentage of Intact [^{11}C]PIB, [^{18}F]**2**, [^{18}F]**3**, and [^{18}F]**6** in Plasma of Normal Rhesus Monkey at 2, 10, 30, and 60 min p.i.[a]

	% intact tracer plasma monkey					
	2 min p.i.	10 min p.i.	30 min p.i.	60 min p.i.	120 min p.i.	180 min p.i.
[^{11}C]PIB	94.9	61.5	62.2	nd	nd	nd
[^{18}F]**2**	91.8	50.6	57.5	62.9	66.3	66.9
[^{18}F]**3**	89.7	42.7	25.1	16.9	17.7	20.8
[^{18}F]**6**	93.5	54.1	24.4	21.1	15.8	nd

[a] $n = 1$ at each time point. nd = not determined.

late images encompass 168−198 min p.i. Also, in the monkey no tracer uptake was observed in the skull for any of the new tracers.

Regions of interest (ROIs; cerebellum, frontal cortex, parietal cortex, pons, thalamus, and white matter) were drawn on the initial (influx-weighted) PET images of the first 20 min p.i., which were coregistered to the monkey's individual volumetric T1 weighted MRI, and the TACs were calculated using PMOD software (Figure 4). These results confirm the high initial brain uptake of [^{18}F]**2** (almost 2 times higher than that of [^{18}F]**6** and [^{11}C]PIB). However, [^{18}F]**3** showed the highest initial brain uptake with a remarkable difference between uptake in the frontal and parietal cortex. [^{11}C]PIB seems to have the most favorable uptake pattern. Its clearance from all indicated brain regions is the fastest indicating that [^{11}C]PIB has the lowest nonspecific binding. A favorable characteristic of [^{18}F]**2** is its fast clearance out of the cerebellum, a region that is often used as reference region. The overall brain kinetics of [^{18}F]**2** seems to be the fastest compared to the other two ^{18}F-labeled phenylbenzothiazoles. The activity ratio between the cerebellum and the white matter (Figure 5) is the highest for [^{18}F]**2**, indicating that this compound may have a lower nonspecific binding in the white matter in comparison with the cerebellum, a favorable characteristic for tracers agents used for in vivo amyloid imaging in AD patients.

Biostability of [^{18}F]2, [^{18}F]3, and [^{18}F]6 in Normal Mice. The in vivo metabolic stability of [^{18}F]**2**, [^{18}F]**3**, and [^{18}F]**6** was studied by HPLC analysis of plasma and brain of normal mice obtained at different time points after iv injection of the ^{18}F-labeled phenylbenzothiazoles. The samples were analyzed on a monolithic C18 column, and the recovery of radioactivity was high (87.0 ± 6.0%, $n = 17$).

An example of plasma analysis of [^{18}F]**2**, [^{18}F]**3**, and [^{18}F]**6** 10 min after injection is shown in Figure 6. Table 7 shows the percentage of intact [^{18}F]KS28, [^{18}F]**2**, [^{18}F]**3**, and [^{18}F]**6** in plasma of normal mice as a function of time postinjection. The data of [^{18}F]KS28 were obtained in a previous study.[26] The fraction of radiometabolites in plasma was the lowest for compound [^{18}F]**2**. Comparison of the percentages of intact [^{18}F]**2** with those of [^{18}F]KS28 demonstrates that [^{18}F]**2** is metabolized to a lesser extent than [^{18}F]KS28. An in vivo metabolic breakdown of [^{18}F]KS28 was suggested as one of the possible reasons for its poor sensitivity as amyloid tracer in AD patients.[14] Figure 6 shows that [^{18}F]**2** is converted to at least two polar metabolites. [^{18}F]**3**, on the other hand, is converted to at least three polar metabolites, one of which was identified as the demethylated derivative of [^{18}F]**3**, namely, [^{18}F]**2**. [^{18}F]**6** is converted to at least four polar metabolites of which two were identified as the mono- and bis-demethylated derivatives [^{18}F]**2** and [^{18}F]**3**. Identification of the radiometabolites was done by co-injection of the nonradioactive reference compounds.

As can be expected, the radiometabolites resulting from demethylation of [^{18}F]**3** and [^{18}F]**6** were also found in the brain (Figure 7). The percentage of brain afctivity in the form of intact [^{18}F]**3** and [^{18}F]**6** was in both cases about 69% at 30 min p.i. and 60% at 60 min p.i. (Table 8). As these metabolites also have high, but different, affinity for human brain amyloid, their presence may complicate the quantification of the PET brain images. For [^{18}F]**2** only relatively low amounts (< 15%) of radiometabolites were found in the brain at 60 min p.i. (86.3% intact [^{18}F]**2**), indicating that no substantial metabolism of [^{18}F]**2** occurs in brain and that its radiometabolites do not cross the BBB to a high extent in mice.

Plasma Radiometabolite Analysis after Injection of [^{18}F]2, [^{18}F]3, and [^{18}F]6 in a Normal Rhesus Monkey. The in vivo metabolic stability of [^{11}C]PIB, [^{18}F]**2**, [^{18}F]**3**, and [^{18}F]**6** was also studied in a rhesus monkey by analyzing plasma samples collected at different time points during the μPET scan (2, 10, 30, 60, 120, or 180 min p.i.). Table 9 shows the percentage of intact [^{11}C]PIB, [^{18}F]**2**, [^{18}F]**3**, and [^{18}F]**6** in plasma of a rhesus monkey as a function of time. Also in this animal

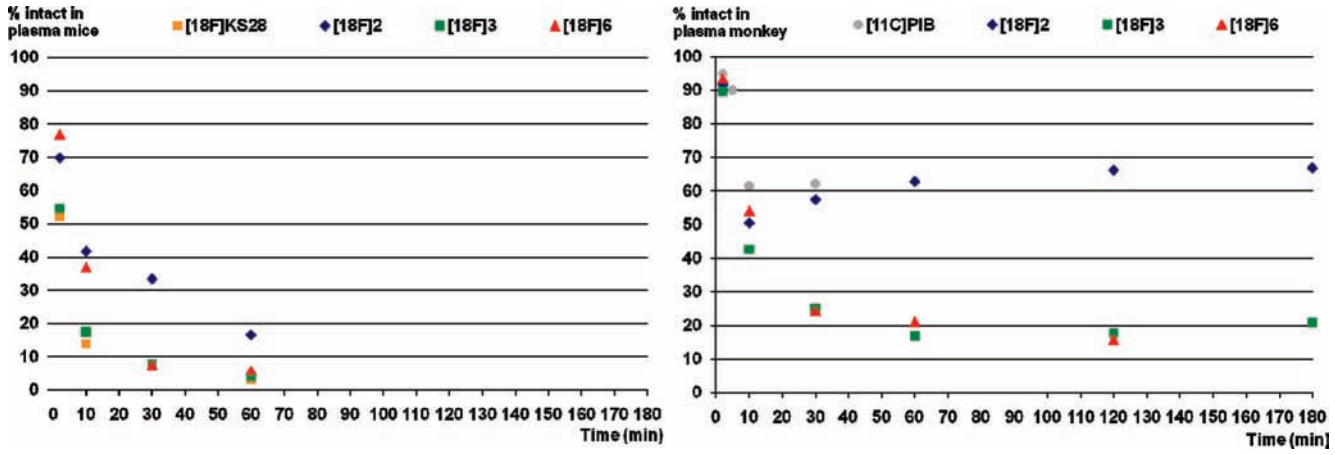

Figure 8. Percentage of intact [^{18}F]KS28, [^{18}F]**2**, [^{18}F]**3**, and [^{18}F]**6** in plasma of normal mice (left) and percentage of intact [^{11}C]PIB, [^{18}F]**2**, [^{18}F]**3**, and [^{18}F]**6** in plasma of normal rhesus monkey (right) as a function of time.

species, [^{18}F]**2** seems to be the most stable agent and its rate of metabolism is comparable with that of [^{11}C]PIB. When the decline in percentage of intact tracer as a function of time is compared between normal mice and the monkey, a slower metabolism is observed in the rhesus monkey (Figure 8).

Conclusion

To allow noninvasive in vivo imaging of amyloid plaques for early stage diagnosis of Alzheimer's disease and monitoring of the disease progression and treatment efficacy with PET, the search for a clinically useful radiolabeled PET tracer is the focus of worldwide research. Up to now, the most promising clinical results have been obtained with [^{11}C]PIB. The limitations associated with the short half-life of carbon-11 may be overcome by introducing a fluorine-18 label, and on the condition of maintenance of favorable biological characteristics, this may provide a tracer agent useful for a widespread clinical application. In a previous study, we evaluated the PIB analogue [^{18}F]KS28 (6-methyl-2-(4′-[^{18}F]fluorophenyl)-1,3-benzothiazole) in two AD patients. Despite the promising preclinical data, this ^{18}F-labeled phenylbenzothiazole showed poor results in a clinical pilot study probably because of its higher nonspecific binding and the slower Aβ binding kinetics in comparison with [^{11}C]PIB.

We have now synthesized and evaluated three new ^{18}F-labeled 2-phenylbenzothiazoles, which all contain a fluorine-18 label directly attached to the 2-phenyl ring and a (methyl substituted) amino group on the benzothiazole part. Such amine substituent is also present in the Pittsburgh compound and in other promising fluorine-18 labeled PET agents, which are under clinical evaluation for diagnosis of AD. The position of the substituent on the amyloid tracers seems to have no influence on the binding characteristics. In 2-phenylbenzothiazoles, an electron-donating amine substituent is supposed to contribute significantly to a specific in vivo binding to amyloid, as it may increase the binding affinity by introducing a positive electrostatic interaction around the sulfur atom of the benzothiazole moiety. All three new 6-amino-2-(4′-fluorophenyl)-1,3-benzothiazoles, with or without methyl substituent(s) on the amine, show high in vitro affinity for amyloid paques present in post mortem human AD brain homogenates ($K_i \leq 10$ nM). The fluorine-18 labeled agents could be obtained in reasonable yields from suitable nitro precursors and were found to pass efficiently the blood−brain barrier in normal mice, rats, and a monkey. Of the new tracer agents, compound [^{18}F]**2** has the highest brain uptake in healthy mice, which is 4 times higher than that of [^{11}C]PIB, and the fastest brain washout. μPET studies in normal rats and a normal rhesus monkey confirmed that [^{18}F]**2** has the most favorable brain kinetics. In addition, this agent seems also to be the most stable in vivo and in a monkey its rate of metabolism in plasma was found to be comparable with that of [^{11}C]PIB. As [^{18}F]**2** cannot be converted to demethylated metabolites, which would also cross the BBB and might complicate quantification of PET brain images, the results of the present study clearly suggest that especially [^{18}F]**2** is a promising candidate as Aβ plaque imaging agent for studying AD patients with PET.

Experimental Section

Chemicals and Reagents. 6-Nitrobenzothiazole was obtained from Alfa Aesar (Karlsruhe, Germany). 1-Bromo-4-fluorobenzene and 1-bromo-4-nitrobenzene were obtained from Acros Organics (Geel, Belgium). All other reagents and solvents were obtained commercially from Acros Organics, Aldrich (Sigma-Aldrich, Bornem, Belgium), Alfa Aesar, Fischer Bioblock Scientific (Tournai, Belgium), Fluka (Bornem, Belgium), Merck (Darmstadt, Germany), or Riedel-de Haën (Seelze, Germany). They were all used without further purification.

Apparatus, Instruments, and General Conditions. $MgSO_4$ was used as drying agent. pH values of nonradioactive solutions were measured with a P600 pH meter (Consort, Turnhout, Belgium) provided with a glass electrode. Evaporation of organic solvents under reduced pressure was done with a Buchi rotovapor (Buchi, Flawil, Switzerland). Purification of reaction mixtures was done by column chromatography using silica gel with a particle size varying between 0.04 and 0.063 mm (230−400 mesh, MN Kieselgel 60M, Macherey-Nagel, Duren, Germany) as the stationary phase. Thin layer chromatography (TLC) was done on precoated silica TLC plates (DC-Alufolien-Kieselgel, Fluka, Buchs, Switzerland). The structure of the synthesized products was confirmed with ^{1}H nuclear magnetic resonance (NMR) spectroscopy on a Gemini 200 MHz spectrometer (Varian, Palo Alto, CA) or a Bruker AVANCE 300 MHz spectrometer (Bruker AG, Faellanden, Switzerland). Chemical shifts are reported as δ-values (parts per million) relative to tetramethylsilane ($\delta = 0$). Coupling constants are reported in hertz. Splitting patterns are defined by s (singlet), d (doublet), dd (double doublet), t (triplet), and m (multiplet). Melting points were determined with an IA9100 digital melting point apparatus (Electrothermal, Essex, U.K.) in open capillaries and are reported uncorrected. Exact mass measurements were performed on a time-of-flight mass spectrometer (LCT, Micromass,

Manchester, U.K.) equipped with an orthogonal electrospray ionization interface, operating in positive mode (ES^+). Accurate mass determination was done by co-injection with a compound with known mass as an internal calibration standard (lock mass). Acquisition and processing of data were done using Masslynx software (version 3.5, Waters, Milford, MA). Purity of the synthesized compounds was determined using analytical high performance liquid chromatography (HPLC) and was found to be more than 95%.

Reversed phase high performance liquid chromatography (RP-HPLC) purification and analysis was performed on a Merck Hitachi L6200 or L7100 or VWR Hitachi L2400 pump (Hitachi, Tokyo, Japan) connected to a UV spectrometer (Waters 2487 dual λ absorbance detector). The output signal was recorded and analyzed using a RaChel data acquisition system (Lablogic, Sheffield, U.K.) or GINA Star data acquisition system (Raytest, Straubenhardt, Germany). For analysis of radiolabeled compounds, the HPLC eluate was led over a 3 in. NaI(Tl) scintillation detector connected to a single channel analyzer (Medi-Lab Select, Mechelen, Belgium) after passage through a UV detector.

Gas chromatography was performed on a DI 200 gas chromatograph (Delsi Instruments, Suresnes, France) with a Porapak QS 80/100 column (Alltech, Deerfield, IL) of 180 cm × 0.25 in.

Animal studies were performed according to the Belgian code of practice for the care and use of animals, after approval from the University Ethics Committee for Animals.

[^{11}C]PIB was synthesized using [^{11}C]methyl triflate following a described procedure.[30]

Quantitative determination of radioactivity in samples was done using an automatic γ-counter coupled to a multichannel analyzer (Wallac 1480 Wizard, 3 in., Wallac, Turku, Finland). The results were corrected for background radiation and physical decay during counting.

Dynamic μPET imaging was performed using a lutetium oxyorthosilicate (LSO) detector-based tomograph (microPET Focus 220; Siemens Medical Solutions, Knoxville, TN), which has a nominal transaxial resolution of 1.35 mm in full width at half-maximum. Data were acquired in a 128 × 128 × 95 matrix with a pixel width of 0.475 mm and a slice thickness of 0.796 mm. The coincidence window width was set at 6 ns. The MRI scan was performed on a Siemens Trio 3T scanner (Siemens Medical Solutions).

Synthesis. 6-Nitro-2-(4′-fluorophenyl)-1,3-benzothiazole (1). A suspension of 6-nitrobenzothiazole (0.218 g, 1.21 mmol), 1-bromo-4-fluorobenzene (0.16 mL, 1.45 mmol), dry cesium carbonate (Cs_2CO_3, 0.394 g, 1.21 mmol), copper(I) bromide (CuBr, 34 mg, 0.24 mmol), palladium(II) acetate ($Pd(OAc)_2$, 13 mg, 0.06 mmol), and tri-*tert*-butylphosphine ($P(t\text{-}Bu)_3$, 24 mg, 0.12 mmol) in 10 mL of dimethylformamide (DMF) was heated at 150 °C under nitrogen while stirring in a sealed tube for 3 h. After cooling to room temperature (rt), the mixture was diluted with ethyl acetate, washed several times with water, and dried on $MgSO_4$ and in a vacuum oven. The residue was purified with silica column chromatography using gradient mixtures of hexane and ethyl acetate (up to 20%) as eluent to yield 0.136 g of **1** as a white solid (0.50 mmol, 41%). ^{1}H NMR ($CDCl_3$-d_6, 200 MHz): δ 7.26 (t, 2H, ^3J = 8.0 Hz, 3′-H 5′-H), 8.14 (d, 2H, ^3J = 8.8 Hz, 2′-H 6′-H), 8.17 (d, 1H, ^3J = 7.7 Hz, 4-H), 8.40 (dd, 1H, ^3J = 9.2 Hz, ^4J = 2.2 Hz, 5-H), 8.86 (d, 1H, ^4J = 2.2 Hz, 7-H). Accurate MS ES^+ m/z $[M + H]^+$ 275.0280 (calculated for $C_{13}H_7N_2O_2FS$ 275.0285). Mp: 176.4−177 °C.

6-Amino-2-(4′-fluorophenyl)-1,3-benzothiazole (2). A solution of **1** (0.100 g, 0.36 mmol) and stannous chloride dihydrate ($SnCl_2 \cdot 2H_2O$, 0.411 g, 1.82 mmol) in dry ethanol (25 mL) was refluxed under nitrogen for 4 h. After the mixture was cooled to room temperature, the ethanol was removed by evaporation under reduced pressure and the residual yellow solid was dissolved in ethyl acetate. The solution was extracted successively with water, 2 M NaOH, and water to remove the tin. The organic phase was dried over $MgSO_4$, filtered, and evaporated to dryness. The obtained yellow oil was purified with silica column chromatography using gradient mixtures of hexane and ethyl acetate (up to 20%) as eluent to yield 78 mg of **2** as a gray powder (0.32 mmol, 89%). ^{1}H NMR ($CDCl_3$-d_6, 200 MHz): δ 3.78 (s, 2H, NH_2), 6.78 (dd, 1H, ^3J = 8.8 Hz, ^4J = 2.6 Hz, 5-H), 7.06 (dd, 2H, ^3J = 5.5 Hz, ^4J = 3.3 Hz, 3′-H 5′-H), 7.19 (s, 1H, 7-H), 7.75 (d, 1H, ^3J = 8.8 Hz, 4-H), 7.93 (dd, 2H, ^3J = 8.8 Hz, ^4J = 5.4 Hz, 2′-H 6′-H). Accurate MS ES^+ m/z $[M + H]^+$ 245.0553 (calculated for $C_{13}H_9N_2FS$ 245.0543). Mp: 145−146 °C.

6-Methylamino-2-(4′-fluorophenyl)-1,3-benzothiazole (3). Method A. To a solution of **2** (37 mg, 0.15 mmol) in methanol (10 mL) was added sodium methoxide (8 mg, 0.15 mmol) and paraformaldehyde (4 mg, 0.15 mmol), and the mixture was refluxed for 2 h. The reaction mixture was cooled to 0 °C, sodium borohydride (5 mg, 0.15 mmol) was added in portions, and the mixture was refluxed further for 1 h. The mixture was then poured into crushed ice and extracted with ethyl acetate. The combined ethyl acetate layers were dried over $MgSO_4$, concentrated, and purified with silica column chromatography using gradient mixtures of hexane and ethyl acetate (up to 30%) as eluent to yield 5 mg of **3** as a yellow solid (0.02 mmol, 13%). ^{1}H NMR ($CDCl_3$, 300 MHz): δ 2.90 (s, 3H, NCH_3), 3.95 (s, 1H, NH), 6.77 (dd, 1H, ^3J = 8.8 Hz, ^4J = 2.2 Hz, 5-H), 6.98 (d, 1H, ^4J = 2.1 Hz, 7-H), 7.14 (t, 2H, ^3J = 8.6 Hz, 3′-H 5′-H), 7.81 (d, 1H, ^3J = 8.8 Hz, 4-H), 7.99 (dd, 2H, ^3J = 8.6 Hz, ^4J = 5.4 Hz, 2′-H 6′-H). Accurate MS ES^+ m/z $[M + H]^+$ 259.0679 (calculated for $C_{14}H_{11}N_2FS$ 259.0700). Mp: 115.4−116.7 °C.

6-Aminobenzothiazole (4). A mixture of 6-nitrobenzothiazole (58.558 g, 0.325 mol) and stannous chloride dihydrate (586.638 g, 2.600 mol) in a mixture of concentrated hydrochloric acid (880 mL) and methanol (880 mL) was refluxed for 30 min. After removal of the methanol by evaporation under reduced pressure, the mixture was poured into crushed ice. The pH of the aqueous solution was adjusted to 10 using 10 M NaOH, and the mixture was extracted with ethyl acetate. The combined ethyl acetate layers were dried over $MgSO_4$ and concentrated to yield 39.055 g of **4** as a yellow solid (0.260 mol, 80%), which was used without further purification. ^{1}H NMR ($CDCl_3$-d_6, 300 MHz): δ 3.86 (s, 2H, NH_2), 6.86 (dd, 1H, ^3J = 8.7 Hz, ^4J = 2.3 Hz, 3-H), 7.15 (d, 1H, ^4J = 2.3 Hz, 7-H), 7.88 (d, 1H, ^3J = 8.7 Hz, 4-H), 8.68 (s, 1H, 2-H). Accurate MS ES^+ m/z $[M + H]^+$ 151.0334 (calculated for $C_7H_6N_2S$ 151.0324). Mp: 86.9−87.4 °C.

6-Dimethylaminobenzothiazole (5). A solution of **4** (30.660 g, 0.203 mol) in tetrahydrofuran (THF, 390 mL) was slowly added to a stirred mixture of 37% formaldehyde (161 mL, 2.030 mol) and 4 M H_2SO_4 (161 mL, 0.608 mol). To the resultant mixture was added powdered iron (90.589 g, 1.622 mol), and the mixture was stirred mechanically for 30 min. The precipitate of iron was removed by filtration and washed with ethyl acetate. The filtrate was made strongly alkaline (pH > 11) with 10% NaOH and was extracted with ethyl acetate. The combined ethyl acetate extracts were dried over $MgSO_4$ and concentrated and the oily residue was purified with silica column chromatography using gradient mixtures of hexane and ethyl acetate (up to 15%) as eluent to yield 1.087 g of **5** as a slightly brown solid (6.10 mmol, 3%). ^{1}H NMR ($CDCl_3$-d_6, 300 MHz): δ 3.02 (s, 6H, $2CH_3$), 6.99 (dd, 1H, ^3J = 9.1 Hz, ^4J = 2.5 Hz, 3-H), 7.14 (d, 1H, ^4J = 2.5 Hz, 7-H), 7.94 (d, 1H, ^3J = 9.0 Hz, 4-H), 8.66 (s, 1H, 2-H). Accurate MS ES^+ m/z $[M + H]^+$ 179.0623 (calculated for $C_9H_{10}N_2S$ 179.0638). Mp: 65.8−66.7 °C.

6-Dimethylamino-2-(4′-fluorophenyl)-1,3-benzothiazole (6). Method B. A mixture of **5** (0.339 g, 1.90 mmol), 1-bromo-4-fluorobenzene (0.25 mL, 2.28 mmol), dry cesium carbonate (0.619 g, 1.90 mmol), copper(I) bromide (55 mg, 0.38 mmol), and palladium(II) acetate (20 mg, 0.09 mmol) in 12 mL of DMF was placed under nitrogen in a sealed tube at 150 °C. Tri-*tert*-butylphosphine (38 mg, 0.19 mmol) was added, and the suspension was stirred for 30 min. The DMF was removed

under reduced pressure and the obtained residue was purified with silica column chromatography using gradient mixtures of hexane and ethyl acetate (up to 15%) as eluent to yield 31 mg of **6** as a slighty yellow solid (0.11 mmol, 6%). ^{1}H NMR ($CDCl_3$, 300 MHz): δ 3.04 (s, 6H, $2CH_3$), 6.96 (dd, 1H, ^3J = 9.0 Hz, ^4J = 2.6 Hz, 5-H), 7.10 (d, 1H, ^4J = 2.5 Hz, 7-H), 7.14 (t, 2H, ^3J = 8.7 Hz, 3′-H 5′-H), 7.88 (d, 1H, ^3J = 9.1 Hz, 4-H), 8.00 (dd, 2H, ^3J = 8.8 Hz, ^4J = 5.3 Hz, 2′-H 6′-H). Accurate MS ES$^+$ m/z $[M + H]^+$ 273.0857 (calculated for $C_{15}H_{13}N_2FS$ 273.0856). Mp: 146.4−147.1 °C.

6-Dimethylamino-2-(4′-nitrophenyl)-1,3-benzothiazole (7). 7 was synthesized following method B starting from **5** (0.713 g, 4.00 mmol), 1-bromo-4-nitrobenzene (0.968 g, 4.79 mmol), dry cesium carbonate (1.304 g, 4.00 mmol), copper(I) bromide (0.114 g, 0.79 mmol), palladium(II) acetate (45 mg, 0.20 mmol), and tri-*tert*-butylphosphine (81 mg, 0.40 mmol) in 24 mL of DMF. Purification with silica column chromatography using gradient mixtures of hexane and ethyl acetate (up to 10%) as eluent and crystallization from ethanol yielded 36 mg of **7** as an orange solid (0.12 mmol, 3%). ^{1}H NMR ($CDCl_3$, 300 MHz): δ 3.08 (s, 6H, $2CH_3$), 7.00 (dd, 1H, ^3J = 9.1 Hz, ^4J = 2.6 Hz, 5-H), 7.10 (d, 1H, ^4J = 2.5 Hz, 7-H), 7.94 (d, 1H, ^3J = 9.1 Hz, 4-H), 8.17 (d, 2H, ^3J = 9.0 Hz, 2′-H 6′-H), 8.31 (d, 2H, ^3J = 9.0 Hz, 3′-H 5′-H). Accurate MS ES$^+$ m/z $[M + H]^+$ 300.0793 (calculated for $C_{15}H_{13}N_3O_2S$ 300.0801). Mp: 230−230.4 °C.

6-*tert*-Butoxycarbonylaminobenzothiazole (8). Method C. To a solution of **4** (0.376 g, 2.50 mmol) in 10 mL of *tert*-butanol at 80 °C were added zinc perchlorate hexahydrate ($Zn(ClO_4)_2 \cdot 6H_2O$, 45 mg, 0.12 mmol) and di-*tert*-butyl dicarbonate ($(BOC)_2O$, 0.709 g, 3.25 mmol), and the mixture was stirred for 3 h. After removal of the *tert*-butanol by evaporation under reduced pressure, the obtained oily residue was purified with silica column chromatography using gradient mixtures of hexane and ethyl acetate (up to 15%) as eluent to yield 0.580 g of **8** as a white oil (2.32 mmol, 93%). ^{1}H NMR ($CDCl_3$-d_6, 300 MHz): δ 1.49 (s, 9H, $C(CH_3)_3$), 7.42 (dd, 1H, ^3J = 8.8 Hz, ^4J = 2.1 Hz, 3-H), 7.85 (d, 1H, ^4J = 2.0 Hz, 7-H), 8.08 (d, 1H, ^3J = 8.8 Hz, 4-H), 8.97 (s, 1H, 2-H). Accurate MS ES$^+$ m/z $[M + H]^+$ 251.0836 (calculated for $C_{12}H_{14}N_2O_2S$ 251.0849).

6-*tert*-Butoxycarbonylamino-2-(4′-nitrophenyl)-1,3-benzothiazole (9). 9 was synthesized following method B starting from **8** (0.576 g, 2.30 mmol), 1-bromo-4-nitrobenzene (0.558 g, 2.76 mmol), dry cesium carbonate (0.749 g, 2.30 mmol), copper(I) bromide (66 mg, 0.46 mmol), palladium(II) acetate (25 mg, 0.11 mmol), and tri-*tert*-butylphosphine (46 mg, 22.80 mmol) in 15 mL of DMF. Purification with silica column chromatography using gradient mixtures of hexane and ethyl acetate (up to 15%) as eluent and crystallization from ethanol yielded 22 mg of **9** as a yellow solid (0.06 mmol, 3%). ^{1}H NMR ($CDCl_3$, 300 MHz): δ 1.56 (s, 9H, $C(CH_3)_3$), 6.69 (s, 1H, 7-H), 7.21 (dd, 1H, ^3J = 6.6 Hz, ^4J = 1.4 Hz, 5-H), 7.99 (d, 1H, ^3J = 6.6 Hz, 4-H), 8.22 (d, 2H, ^3J = 6.5 Hz, 2′-H 6′-H), 8.34 (d, 2H, ^3J = 6.6 Hz, 3′-H 5′-H). Accurate MS ES$^+$ m/z $[M + H]^+$ 372.4250 (calculated for $C_{18}H_{17}N_3O_4S$ 372.4247). Mp: 200.4−201.3 °C.

6-*tert*-Butoxycarbonylmethylamino-2-(4′-nitrophenyl)-1,3-benzothiazole (12). 12 was synthesized following method B starting from **11** (5.290 g, 20.00 mmol), 1-bromo-4-nitrobenzene (4.840 g, 24.00 mmol), dry cesium carbonate (6.520 g, 20.00 mmol), copper(I) bromide (0.598 g, 3.96 mmol), palladium(II) acetate (0.223 g, 0.99 mmol), and tri-*tert*-butylphosphine (0.401 g, 1.98 mmol) in 120 mL of DMF. Purification with silica column chromatography using gradient mixtures of hexane and ethyl acetate (up to 15%) as eluent and crystallization from ethanol yielded 1.670 g of 12 as a yellow solid (4.33 mmol, 22%). ^{1}H NMR ($CDCl_3$, 300 MHz): δ 1.49 (s, 9H, $C(CH_3)_3$), 3.36 (s, 3H, NCH_3), 7.45 (dd, 1H, ^3J = 8.8 Hz, ^4J = 1.8 Hz, 5-H), 7.85 (s, 1H, 7-H), 8.05 (d, 1H, ^3J = 8.8 Hz, 4-H), 8.24 (d, 2H, ^3J = 8.8 Hz, 2′-H 6′-H), 8.35 (d, 2H, ^3J = 8.7 Hz, 3′-H 5′-H). Accurate MS ES$^+$ m/z $[M + H]^+$ 386.1167 (calculated for $C_{19}H_{19}N_3O_4S$ 386.1169). Mp: 138.6−139.2 °C.

Production of [^{18}F]Fluoride and Radiosynthesis of 6-Amino-2-(4′-[^{18}F]fluorophenyl)-1,3-benzothiazole ([^{18}F]2, 6-Methylamino-2-(4′-[^{18}F]fluorophenyl)-1,3-benzothiazole ([^{18}F]3, and 6-Dimethylamino-2-(4′-[^{18}F]fluorophenyl)-1,3-benzothiazole ([^{18}F]6. [^{18}F]Fluoride was produced via a [^{18}O(p,n)^{18}F] reaction by irradiation of 0.5−2.0 mL of 97% enriched $H_2{}^{18}O$ (Rotem HYOX^{18}, Rotem Industries, Beer Sheva, Israel) in a niobium target using 18 MeV protons from a Cyclone 18/9 cyclotron (Ion Beam Applications, Louvain-la-Neuve, Belgium). The aqueous solution of [^{18}F]F^- was transferred to a synthesis module where [^{18}F]F^- was separated from $H_2{}^{18}O$ using a Sep-Pak Light Waters Accell Plus CM cartridge (Waters). [^{18}F]F^- was then eluted from the cartridge into a reaction vial with a solution containing 2.5 mg of potassium carbonate and 27.9 mg of Kryptofix 2.2.2 dissolved in 0.75 mL of water/acetonitrile (5:95 v/v). After evaporation of the solvent from the reaction vial under a stream of helium at 115 °C for 7 min, [^{18}F]F^- was further dried by azeotropic distillation of traces of water using 1 mL of anhydrous acetonitrile (115 °C, 5 min). A solution of 1.5 mg of precursor in 0.5 mL of anhydrous DMSO was added to the radioactive residue of K[^{18}F]F-Kryptofix, and the mixture was heated at 150 °C for 20 min in a closed vial to provide the crude radiolabeled compound. For the synthesis of 6-amino-2-(4′-[^{18}F]fluorophenyl)-1,3-benzothiazole ([^{18}F]**2**) and 6-methylamino-2-(4′-[^{18}F]fluorophenyl)-1,3-benzothiazole ([^{18}F]**3**), 0.3 mL of 1 M HCl was added after the radiolabeling reaction and the mixture was heated at 100 °C for 5 min. To neutralize the reaction mixture, 0.4 mL of 0.5 M Na_2HPO_4 was added. The crude mixtures were applied onto an XTerra Prep RP_{18} 10 mm × 250 mm column (Waters) that was eluted with an isocratic mixture of 45% 0.05 M NH_4OAc and 55% ethanol/tetrahydrofuran (75:25 v/v) at a flow rate of 3 mL/min. Radiolabeled 6-amino-2-(4′-[^{18}F]fluorophenyl)-1,3-benzothiazole ([^{18}F]**2**), 6-methylamino-2-(4′-[^{18}F]fluorophenyl)-1,3-benzothiazole ([^{18}F]**3**), and 6-dimethylamino-2-(4′-[^{18}F]fluorophenyl)-1,3-benzothiazole ([^{18}F]**6**) were collected at 20, 16, and 22 min, respectively. Their corresponding precursors **9**, **12**, and **7** eluted at 26, 20, and 28 min, respectively. The fractions containing the isolated radioactive compound were diluted with an equal volume of water and were then applied on an activated Sep-Pak Plus C18 cartridge (Waters) that was first rinsed with water and then eluted with 1 mL of ethanol. The purity of [^{18}F]**2** was analyzed using an XTerra RP_{18} 3.5 μm, 3.0 mm × 100 mm column (Waters) eluted with an isocratic mixture of 60% 0.05 M NH_4OAc and 40% ethanol/tetrahydrofuran (75:25 v/v) and after 5 min with an isocratic mixture of 40% 0.05 M NH_4OAc and 60% ethanol/tetrahydrofuran (75:25 v/v) at a flow rate of 0.35 mL/min (t_R([^{18}F]**2**) = 7.5 min). For purity analysis of [^{18}F]**3** and [^{18}F]**6**, the same column was eluted with an isocratic mixture of 55% 0.05 M NH_4OAc and 45% ethanol/tetrahydrofuran (75:25 v/v) or 45% 0.05 M NH_4OAc and 55% ethanol/tetrahydrofuran (75:25 v/v), respectively, at a flow rate of 0.35 mL/min (t_R([^{18}F]**3**) = 12 min and t_R([^{18}F]**6**) = 7.5 min). Decay corrected radiochemical yields, corrected for the fraction of [^{18}F]fluoride retained on the Sep-Pak Light Accell plus QMA anion exchange cartridge, were 10.5 ± 5.2% for [^{18}F]**2**, 45.0 ± 12.5% for [^{18}F]**3**, and 19.3 ± 9.0% for [^{18}F]**6**. The overall synthesis time to obtain the pure products was between 75 and 100 min. The average specific activity was found to be 72 GBq/μmol for [^{18}F]**2**, 82 GBq/μmol for [^{18}F]**3**, and 24 GBq/μmol for [^{18}F]**6** at the end of synthesis.

Binding Studies. Binding studies were carried out according to a method described previously.[27] [^{125}I]IMPY (6-[^{125}I]iodo-2-(4′-dimethylamino)phenyl-imidazo[1,2]pyridine) with a specific activity of 81.4 TBq/mmol and greater than 95% radiochemical purity was prepared using a standard iododestannylation reaction and purified using a simplified C-4 minicolumn. Binding assays were carried out in 12 mm × 75 mm borosilicate glass tubes. The reaction mixture contained 50 μL of post mortem AD brain homogenate (20−50 μg), 50 μL of [^{125}I]IMPY

solution (0.04−0.06 nM diluted in phosphate buffered saline (PBS)), and 50 μL of solutions of the test compound (10^{-5}−10^{-10} M diluted serially in PBS containing 0.1% bovine serum albumin) in a final volume of 1 mL. Nonspecific binding was defined in the presence of 600 nM nonradioactive IMPY in the same assay tubes. The mixtures were incubated at 37 °C for 2 h, and the bound and free radioactivity were separated by vacuum filtration through Whatman GF/B filters using a Brandel M-24R cell harvester (Brandel, Gaithersburg, MD) followed by two 3 mL washes with PBS at room temperature. Filters containing the bound iodine-125 labeled ligand were counted in a γ counter with 70% counting efficacy. Under the assay conditions, the specifically bound fraction was less than 15% of total radioactivity. The results of inhibition experiments were subjected to nonlinear regression analysis using EBDA,[31] from which K_i values were calculated.

Partition Coefficient Determination. The lipophilicity of the RP-HPLC isolated ^{18}F-complexes was determined using a modification of the method described by Yamauchi and co-workers.[32] A 25 μL aliquot of the RP-HPLC isolated solution of the ^{18}F-labeled compound was added to a tube containing 2 mL of 1-octanol and 2 mL of 0.025 M phosphate buffer, pH 7.4 (n = 6). The test tube was vortexed at room temperature for 3 min followed by centrifugation at 3000 rpm (1837 g) for 10 min (Eppendorf centrifuge 5810, Eppendorf, Westbury, NY). Aliquots of 61 and 500 μL were drawn from the 1-octanol and buffer phases, respectively, taking care to avoid cross-contamination between the two phases and weighed. The radioactivity in the aliquots was counted using an automatic γ counter. After correction for density and mass difference between the two phases, the partition coefficient (P) was calculated using the following equation:

$$P = \frac{\text{cpm/(mL of octanol)}}{\text{cpm/(mL of buffer)}}$$

with cpm = counts per minute.

Biodistribution in Normal Mice. A solution of [^{18}F]**2**, [^{18}F]**3**, or [^{18}F]**6** obtained after RP-HPLC purification was diluted using 0.9% NaCl in water for injection to a concentration of 3.7 MBq/mL. The concentration of ethanol in the final preparation did not exceed 10% and the concentration of THF did not exceed 0.02%, as determined by gas chromatography. Biodistribution was studied in male NMRI mice (body mass 30−40 g). The mice were anesthetized with isoflurane (1.5−2.5%) in oxygen at a flow rate of 1−2 L/min, and an aliquot of 0.1 mL of the diluted tracer solution was injected via a tail vein. The mice were sacrificed by decapitation at 2 or 60 min p.i. Blood was collected in a tared tube and weighed. All organs and other body parts were dissected and weighed, and their radioactivity was counted in a γ counter. Results were corrected for background radioactivity and are expressed as percentage of the injected dose (% ID), percentage of the injected dose per gram tissue (% ID/g), or standard uptake value (SUV). SUVs were calculated as (radioactivity in cpm in organ/weight of the organ)/(total counts recovered/body weight). For calculation of total radioactivity in blood, blood mass was assumed to be 7% of the total body mass.

***μ*PET Study in a Normal Rat.** A male Wistar rat (500 g) was anesthetized with isoflurane (1.5−2.5%) in oxygen at a flow rate of 1−2 L/min and was injected with 28.5 MBq [^{18}F]**2**, 17.3 MBq [^{18}F]**3**, or 20.4 MBq [^{18}F]**6** via a tail vein with a time interval of 1 or 3 days between each tracer injection. The rat was also injected with 29.0 MBq [^{18}F]**2** 30 min after intraperitoneal injection of 0.35 mg of reference compound **2** and was breathing spontaneously throughout the entire experiment. Dynamic μPET images were acquired for 120 min (4 × 15 s, 4 × 60 s, 5 × 180 s, 8 × 300 s, 10 × 360 s), and reconstruction was done using filtered back projection with a RAMP filter. Data were analyzed using PMOD2.7 software (Zurich, Switzerland), volumes of interest (VOIs) were defined on the summed images, and time−activity curves (TACs) were drawn. In a previous study[26] another rat was injected with 35.3 MBq [^{11}C]PIB and 6.2 MBq [^{18}F]KS28 and dynamic μPET images were acquired for 90 min (4 × 15 s, 4 × 60 s, 5 × 180 s, 14 × 300 s) and 120 min (4 × 15 s, 4 × 60 s, 5 × 180 s, 8 × 300 s, 6 × 600 s), respectively.

***μ*PET Study in a Normal Rhesus Monkey.** One juvenile male rhesus monkey (maccaca mulatta, 5.0 kg) was sedated with ketamine (Ketalar) and xylazine (Rompun) (intramuscular injection) and anesthetized during the μPET experiment with isoflurane (1.0−1.5%). The blood concentration of O_2 and CO_2, the breathing frequency, and heartbeat were monitored during the entire experiment. The monkey was injected with 109.4 MBq [^{18}F]**2**, 81.2 MBq [^{18}F]**3**, 96.3 MBq [^{18}F]**6**, or 152.9 MBq [^{11}C]PIB via the vena saphena with a time interval of 1 day between each tracer injection. Dynamic μPET images were acquired for 180 min (5 × 60 s, 5 × 120 s, 9 × 300 s, 12 × 600 s) for [^{18}F]**2**, [^{18}F]**3**, and [^{18}F]**6** and for 90 min (5 × 60 s, 5 × 120 s, 9 × 300 s, 3 × 600 s) for [^{11}C]PIB. Reconstruction of the images and data analysis were performed in the same way as described for the μPET study in a normal rat.

Plasma Radiometabolite Analysis after Injection of [^{18}F]2, [^{18}F]3, and [^{18}F]6 in Normal Mice. After intravenous injection of about 9 MBq of [^{18}F]**2**, [^{18}F]**3**, or [^{18}F]**6** via a tail vein, normal male NMRI mice were sacrificed by decapitation at 2, 10, 30, or 60 min p.i. (n = 3 at each time point). Blood was collected into a BD vacutainer (containing 7.2 mg of K_2EDTA; BD, Franklin Lakes, NJ). The samples were centrifuged at 3000 rpm (1837g) for 5 min at 4 °C (Eppendorf centrifuge 5810) to separate plasma. The supernatant plasma sample was mixed with 25 μL of solution containing the authentic nonradioactive **2**, **3**, or **6** (1 mg/mL acetonitrile), and 200 μL of the mixture was injected onto a Chromolith Performance RP-18 column (3 mm × 100 mm, Merck) eluted with a gradient mixture of 0.05 M ammonium acetate/acetonitrile (0 min, 2:98 v/v; 2 min, 2:98 v/v; 12 min, 40:60 v/v; 17 min, 40:60 v/v; 22 min, 98:2 v/v; 25 min, 98:2 v/v) at a flow rate of 1 mL/min. After passage through an in-line UV detector (254 nm), the HPLC eluate was collected in 1 mL fractions and their radioactivity was measured using a γ counter.

Brain Radiometabolite Analysis after Injection of [^{18}F]2, [^{18}F]3, and [^{18}F]6 in Normal Mice. After intravenous injection of about 9 MBq of [^{18}F]**2**, [^{18}F]**3**, or [^{18}F]**6** via a tail vein, normal male NMRI mice (n = 3) were sacrificed by decapitation at 2, 10, 30, or 60 min p.i. The brain was removed, 100 μL of solution containing the authentic nonradioactive **2**, **3**, or **6** (1 mg/mL acetonitrile), 2 mL of acetonitrile, and 2 mL of water were added, and the mixture was homogenized. After centrifugation at 3000 rpm (1837g) for 5 min at 4 °C (Eppendorf centrifuge 5810), 1 mL of supernatant was filtered (0.22 μm pore size/10 mm diameter) and the filtrate was analyzed on an XTerra RP C18 column (5 μm, 4.6 mm × 250 mm) eluted with a mixture of 0.05 M ammonium acetate/acetonitrile ([^{18}F]**2**, 60:40 v/v at a flow rate of 1.2 mL/min; [^{18}F]**3**, 50:50 v/v at a flow rate of 1.5 mL/min; [^{18}F]**6**, 45:55 v/v at a flow rate of 1.5 mL/min). After passage through an in-line UV detector (254 nm), the HPLC eluate was collected in 1 min fractions and their radioactivity was measured using a γ counter.

Plasma Radiometabolite Analysis after Injection of [^{18}F]2, [^{18}F]3, and [^{18}F]6 in a Normal Rhesus Monkey. Blood was collected during the μPET scan via vena saphena at different time points after injection (2, 10, 30, 60, 120, or 180 min p.i.), and samples were analyzed in the same way as described for plasma radiometabolite analysis in normal mice.

Acknowledgment. This study was funded in part by the EC-FP6-Project DiMI, LSHB-CT-2005-512146.

Supporting Information Available: Experimental details for **10** and **11** and additional data from ^{1}H NMR, MS, and HPLC

analyses for the synthesized final products. This material is available free of charge via the Internet at http://pubs.acs.org.

References

(1) Selkoe, D. J. Alzheimer's disease: genes, proteins, and therapy. *Phys. Rev.* **2001**, *81*, 741–766.
(2) Selkoe, D. J. Cell biology of protein misfolding: the examples of Alzheimer's and Parkinson's diseases. *Nat. Cell Biol.* **2004**, *6*, 1054–1061.
(3) Hardy, J.; Selkoe, D. J. The amyloid hypothesis of Alzheimer's disease: progress and problems on road to therapeutics. *Science* **2002**, *297*, 353–356.
(4) Sano, M.; Grossman, H.; Van Dyk, K. Preventing Alzheimer's disease: separating fact from fiction. *CNS Drugs* **2008**, *22*, 887–902.
(5) Klunk, W. E.; Engler, H.; Nordberg, A.; Wang, Y.; Blomqvist, G.; Holt, D.; Bergstrom, M.; Savitcheva, I.; Huang, G.; Estrada, S.; Ausén, B.; Debnath, M.; Barletta, J.; Price, J. C.; Sandell, J.; Lopresti, B.; Wall, A.; Koivisto, P.; Antoni, G.; Mathis, C.; Langstrom, B. Imaging brain amyloid in Alzheimer's disease with Pittsbugh compound-B. *Ann. Neurol.* **2004**, *55*, 306–319.
(6) Archer, H.; Edison, P.; Brooks, D.; Barnes, J.; Frost, C.; Yeatman, T.; Fox, N.; Rossor, M. Amyloid load and cerebral atrophy in Alzheimer's disease: an ^{11}C-PIB positron emission tomography study. *Ann. Neurol.* **2006**, *60*, 145–147.
(7) Suemoto, T.; Okamura, N.; Shiomitsu, T.; Suzuki, M.; Shimadzu, H.; Akatsu, H.; Yamamoto, T.; Kudo, Y.; Sawada, T. In vivo labeling of amyloid with BF-108. *Neurosci. Res.* **2004**, *48*, 65–74.
(8) Zhang, W.; Oya, S.; Kung, M. P.; Hou, C.; Maier, D.; Kung, H. F. F-18 Polyethyleneglycol stilbenes as PET imaging agents targeting Aβ aggregates in the brain. *Nucl. Med. Biol.* **2005**, *32*, 799–809.
(9) Chang, Y.; Jeong, J.; Lee, Y. S.; Kim, H.; Rai, G.; Kim, Y.; Lee, D.; Chung, J. K.; Lee, M. Synthesis and evaluation of benzothiophene derivatives as ligands for imaging β-amyloid plaques in Alzheimer's disease. *Nucl. Med. Biol.* **2006**, *33*, 811–820.
(10) Zhuang, Z. P.; Kung, M. P.; Kung, H. F. Synthesis of biphenyltrienes as probes for β-amyloid plaques. *J. Med. Chem.* **2006**, *49*, 2841–2844.
(11) Sato, K.; Higuchi, M.; Iwata, N.; Saido, T.; Sasamoto, K. Fluoro-substituted and ^{13}C-labeled styrylbenzene derivatives for detecting brain amyloid plaques. *Eur. J. Med. Chem.* **2004**, *39*, 573–578.
(12) Zhuang, W.; Kung, M. P.; Oya, S.; Hou, C.; Kung, H. F. ^{18}F-Labeled styrylpyridines as PET agents for amyloid plaque imaging. *Nucl. Med. Biol.* **2007**, *34*, 89–97.
(13) Ryu, E.; Choe, Y.; Lee, K. H.; Choi, Y.; Kim, B. T. Curcumin and dehydrozingerone derivatives: synthesis, radiolabelling, and evaluation for β-amyloid plaque imaging. *J. Med. Chem.* **2006**, *49*, 6111–6119.
(14) Serdons, K.; Bormans, G.; Vandenberghe, R.; Koole, M.; Dupont, P.; Vandenbulcke, M.; Nelissen, N.; Thierens, H.; Sciot, R.; Verbruggen A.; Van Laere, K. Toxicity studies, biodistribution, radiation dosimetry and clinical evaluation of the amyloid imaging agent [^{18}F]KS28. *Q. J. Nucl. Med. Mol. Imaging*, submitted.
(15) Small, G.; Kepe, V.; Ercoli, L.; Siddarth, P.; Bookheimer, S.; Miller, K.; Lavretsky, H.; Burggren, A.; Cole, G.; Vinters, H.; Thompson, P.; Huang, S. C.; Satyamurthy, N.; Phelps, M.; Barrio, J. PET of brain amyloid and tau in mild cognitive impairment. *N. Engl. J. Med.* **2006**, *355*, 2652–2663.
(16) Rowe, C. C.; Ackerman, U.; Browne, W.; Mulligan, R.; Pike, K. L.; O'Keefe, G.; Tochon-Danguy, H.; Chan, G.; Berlangieri, S. U.; Jones, G.; Dickinson-Rowe, K. L.; Kung, H. P.; Zhang, W.; Kung, M. P.; Skovronsky, D.; Dyrks, T.; Holl, G.; Krause, S.; Friebe, M.; Lehman, L.; Lindemann, S.; Dinkelborg, L. M.; Masters, C. L.; Villemagne, V. L. Imaging of amyloid β in Alzheimer's disease with ^{18}F-BAY94-9172, a novel PET tracer: proof of mechanism. *Lancet Neurol.* **2008**, *7*, 129–135.
(17) Mathis, C.; Lopresti, B.; Mason, N.; Price, J.; Flatt, N.; Bi, W.; Ziolko, S.; DeKosky, S.; Klunk, W. Comparison of the amyloid imaging agents [F-18]3′-F-PIB and [C-11]PIB in Alzheimer's disease and control subjects. *J. Nucl. Med.* **2007**, *48*, 56P.
(18) Koole, M.; Lewis, D. M.; Buckley, C.; Nelissen, N.; Vandenbulcke, M.; Brooks, D. J.; Vandenberghe, R.; Van Laere, K. Whole-body biodistribution and radiation dosimetry of ^{18}F-GE067, a radioligand for in vivo brain amyloid imaging. *J. Nucl. Med.* **2009**, *50*, 818–822.
(19) Kim, M. K.; Choo, I. H.; Lee, H. S.; Woo, L. I.; Chong, Y. 3D-QSAR of PET agents for imaging β-amyloid in Alzheimers' disease. *Bull. Korean Chem. Soc.* **2007**, *28*, 1231–1234.
(20) Alagille, D.; Baldwin, R. M.; Tamagan, G. D. One-step synthesis of 2-arylbenzothiazole ('BTA') and -benzoxazole precursors for in vivo imaging of β-amyloid plaques. *Tetrahedron Lett.* **2005**, *46*, 1349–1351.
(21) Chandra, R.; Oya, S.; Kung, M.-P.; Hou, C.; Jin, L.-W.; Kung, H. F. New diphenylacetylenes as probes for positron emission tomgraphic imaging of amyloid plaques. *J. Med. Chem.* **2007**, *50*, 2415–2423.
(22) Caléta, I.; Cetina, M.; Hergold-Brundic, A.; Nagl, A.; Karminski-Zamola, G. Synthesis and crystal structure determination of 6-(*N*-isopropyl)amidino-2-methylbenzothiazole hydrochloride monohydrate and 2-amino-6-(*N*-isopropyl)amidinobenzothiazole hydrochloride. *Struct. Chem.* **2003**, *14*, 587–595.
(23) Hrobarik, P.; Sigmundova, I.; Zahradnik, P. Preparation of novel push−pull benzothiazole derivatives with reverse polarity: compounds with potential non-linear optic application. *Synthesis* **2005**, *4*, 600–604.
(24) Bartoli, G.; Bosco, M.; Locatelli, M.; Marcantoni, E.; Massaccesi, M.; Melchiorre, P.; Sambri, L. A Lewis acid-mediated protocol for the protection of aryl amines as their Boc-derivatives. *Synlett* **2004**, *10*, 1794–1798.
(25) Serdons, K.; Verduyckt, T.; Vanderghinste, D.; Cleynhens, J.; Borghgraef, P.; Vermaelen, P.; Terwinghe, C.; Van Leuven, F.; Van Laere, K.; Kung, H.; Bormans, G.; Verbruggen, A. Synthesis of ^{18}F-labelled 2-(4′-fluorophenyl)-1,3-benzothiazole and evaluation as amyloid imaging agent in comparison with [^{11}C]PIB. *Bioorg. Med. Chem. Lett.* **2009**, *19*, 602–605.
(26) Serdons, K.; Terwinghe, C.; Vermaelen, P.; Van Laere, K.; Kung, H. F.; Mortelmans, L.; Bormans, G.; Verbruggen, A. Synthesis and evaluation of ^{18}F-labeled 2-phenylbenzothiazoles as positron emission tomography agents for amyloid plaques in Alzheimer's disease. *J. Med. Chem.* **2009**, *52*, 1428–1437.
(27) Kung, M. P.; Hou, C.; Zhuang, Z. P.; Skovronsky, D.; Kung, H. F. Binding of two potential imaging agents targeting amyloid plaques in postmortem brain tissues of patients with Alzheimer's disease. *Brain Res.* **2004**, *1025*, 89–105.
(28) Dishino, D.; Welch, M.; Kilbourn, M.; Raichle, M. Relationship between lipophilicity and brain extraction of C-11-labeled radiopharmaceuticals. *J. Nucl. Med.* **1983**, *24*, 1030–1038.
(29) Serdons, K.; Verduyckt, T.; Vanderghinste, D.; Borghgraef, P.; Cleynhens, J.; Van Leuven, F.; Kung, H.; Bormans, G.; Verbruggen, A. ^{11}C-labelled PIB analogues as potential tracer agents for in vivo imaging of amyloid β in Alzheimer's disease. *Eur. J. Med. Chem.* **2009**, *44*, 1415–1426.
(30) Solbach, C.; Uebele, M.; Reischl, G.; Machulla, H.-J. Efficient radiosynthesis of carbon-11 labelled uncharged thioflavin T derivatives using [^{11}C]methyl triflate for β-amyloid imaging in Alzheimer's disease with PET. *Appl. Radiat. Isot.* **2005**, *62*, 591–595.
(31) Munson, P. J.; Rodbard, D. Ligand: a versatile computerized approach for characterisation of ligand-binding systems. *Anal. Biochem.* **1980**, *107*, 220–239.
(32) Yamauchi, H.; Takahashi, J.; Seri, S.; Kawashima, H.; Koike, H.; Kato-Azuma, M. In *Technetium and Rhenium in Chemistry and Nuclear Medicine*; Nicolini, M., Bandoli, G., Mazzi, U., Eds.; Cortina International: Verona, Italy, 1989; Vol. 3, pp 475−502.